Interionic Structure of Ion Pairs and Ion Quadruples of Half-Sandwich Ruthenium(II) Salts Bearing α-Diimine Ligands

Daniele Zuccaccia,[†] Gianfranco Bellachioma,[†] Giuseppe Cardaci,[†] Gianluca Ciancaleoni,[†] Cristiano Zuccaccia,[†] Eric Clot,*[,‡] and Alceo Macchioni*[,†]

Dipartimento di Chimica, Università degli Studi di Perugia, Via Elce di Sotto 8, 06123 Perugia, Italy, and Institut Charles Gerhardt Université Montpellier 2 and CNRS, Case Courrier 1501, Place Eugéne Bataillon, 34095 Montpellier Cedex 5, France

Received April 2, 2007

The interionic structure of complexes [Ru(η^6-Arene){(2-R-C_6H_4)N═C(Me)−C(Me)═N(2-R-C_6H_4)}-Cl]X was investigated by an integrated experimental (PGSE diffusion and NOE NMR spectroscopy and X-ray single-crystal studies) and theoretical (DFT and ONIOM calculations) approach. PGSE NMR experiments indicated that ion pairing is the main aggregative process in CD_2Cl_2 and solvents with higher relative permittivity. They also showed that the tendency to ion pairing for isodielectric solvents is higher when the latter are protic. NOE interionic contacts were observed in 2-propanol-d_8 even for $BARF^-$ salts. Ion pairing was favored by more coordinating counterions and an increase in concentration. An equilibrium between ion pairs and ion quadruples was observed by PGSE measurements in chloroform-*d* and benzene-d_6. Such equilibrium is shifted toward ion quadruples by an increase in the concentration or when least coordinating counterions are used. For small fluorinated counterions, NOE studies located the anion in ion pairs above the plane containing the C═N imine moieties. ONIOM calculations found that this anion−cation orientation was at least 35.9 kJ/mol lower in energy than a second orientation with the anion close to cymene, which, in some cases, was observed in the solid state. NOE investigations on complexes with BPh_4^- counterion did not allow a single orientation capable of explaining the observed NOEs to be found. X-ray studies showed that one cation is surrounded by two anions. ONIOM calculations found that these two anion−cation orientations have similar energies. X-ray and NOE NMR data strongly suggest that ion quadruples with BPh_4^- anions are constituted by an alternation of cations and anions. Interionic NOE intensities are almost invariant on passing from ion pairs to ion quadruples with small fluorinated counterions. X-ray studies suggested at least four possible structures of ion quadruples differing in both disposition and orientation of the ionic moieties. Three structures considered by ONIOM calculations were similar in energy, but more stable than the separated ion pairs.

Introduction

The ion-pairing[1] phenomenon plays a crucial role in transition-metal chemistry.[2,3] Many chemical reactions are mediated by ionic (very often cationic) transition-metal complexes, and a proper choice of counterion and solvent is critical in order to maximize activity and selectivity.[2] A particularity of transition-metal ion pairs is that the counterion can occupy one of the coordinating sites or remain in the second coordination sphere, affording inner-sphere ion pairs (ISIPs) or outer-sphere ion pairs (OSIPs), respectively.[2] In favorable conditions, i.e., elevated concentration in solvents with low relative permittivity, OSIPs may aggregate, forming ion quadruples.[4,5] The formation of the latter can be facilitated by the establishment of "inter-ion-pair" hydrogen bonds[6] or $\pi-\pi$ stacking interactions.[7,8] Looking at ion pairs as globally neutral species, the association of two ion pairs to form an ion quadruple differs little from the association of two neutral and polarized molecules to form a dimer.[9]

It would be extremely important to correlate the structure of ion pairs and ion quadruples in solution with their reactivity. In recent years the interionic structure of several transition-metal complex ion pairs has been determined by means of NOE (nuclear Overhauser effect)[10] and PGSE (pulsed field gradient spin−echo)[11] NMR experiments, but a clear correlation with their reactivity has been found only in a few cases.[12,13] On the other hand, almost nothing is known about the interionic structure of ion quadruples in solution.

Herein we report the interionic structure of ion pairs and ion quadruples of [Ru(η^6-Arene){(2-R-C_6H_4)N═C(Me)−C(Me)═N(2-R-C_6H_4)}Cl]X complexes[14] investigated through an inte-

* Corresponding authors. E-mail: clot@univ-montp2.fr; alceo@unipg.it.
[†] Università degli Studi di Perugia.
[‡] Université Montpellier 2.

(1) Marcus, Y.; Hefter, G. *Chem. Rev.* **2006**, *106*, 4585−4621.
(2) Macchioni, A. *Chem. Rev.* **2005**, *105*, 2039−2073, and references therein.
(3) Chen, E. Y.-X.; Marks, T. *J. Chem. Rev.* **2000**, *100*, 1391. Bochmann, M. *J. Organomet. Chem.* **2004**, *689*, 3982.
(4) Beck, S.; Geyer, A.; Brintzinger, H.-H. *Chem. Commun.* **1999**, 2477−2478.
(5) Zuccaccia, C.; Stahl, N. G.; Macchioni, A.; Chen, M.-C.; Roberts, J. A.; Marks, T. J. *J. Am. Chem. Soc.* **2004**, *126*, 1448−1464. Song, F.; Lancaster, S. J.; Cannon, R. D.; Schormann, M.; Humphrey, S. M.; Zuccaccia, C.; Macchioni, A.; Bochmann, M. *Organometallics* **2005**, *24*, 1315−1328.
(6) Zuccaccia, D.; Macchioni, A. *Organometallics* **2005**, *24*, 3476−3486.
(7) Macchioni, A.; Romani, A.; Zuccaccia, C.; Guglielmetti, G.; Querci, C. *Organometallics* **2003**, *22*, 1526. Zuccaccia, D.; Bellachioma, G.; Cardaci, G.; Zuccaccia, C.; Macchioni, A. *Dalton Trans.* **2006**, 1963.
(8) Hamidov, H.; Jeffery, J. C.; Lynam, J. M. *Chem. Commun.* **2004**, 1364.
(9) Zuccaccia, D.; Clot, E.; Macchioni, A. *New J. Chem.* **2005**, *29*, 430−433.
(10) Macchioni, A. *Eur. J. Inorg. Chem.* **2003**, 195, and references therein.

10.1021/om7003157 CCC: $37.00
Publication on Web 06/23/2007

Scheme 1

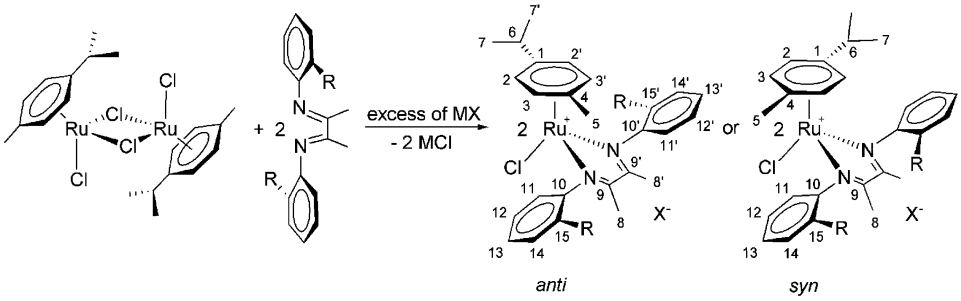

grated experimental and theoretical approach based on NOE and PGSE NMR, X-ray, and DFT and ONIOM calculations. This approach allowed an in-depth evaluation of the presence and structure of ion pairs and ion quadruples in solution as a function of the counterion and solvent, and the energetics of ion quadruple formation from the association of two ion pairs.

Results

Synthesis. [Ru(η^6-Arene){(2-R-C_6H_4)N=C(Me)−C(Me)=N(2-R-C_6H_4)}Cl]X complexes {**1**X, Arene = *p*-cymene, R = H, X = BF_4^-, PF_6^-, BPh_4^-, and $BARF^-$ [B(3,5-$(CF_3)_2$-$C_6H_3)_4^-$]; **2**X *syn* and *anti*, Arene = *p*-cymene, R = Me, X = BF_4^-, and BPh_4^-; **3**X *syn* and *anti*, Arene = *p*-cymene, R = Et, X = BF_4^-, PF_6^-, BPh_4^-, and $CF_3SO_3^-$; **4**X *syn* and *anti*, Arene = *p*-cymene, R = *i*-Pr, X = BF_4^-, PF_6^-, and BPh_4^-; **5**X, Arene = benzene, R = H, X = PF_6^- and BPh_4^-} were synthesized by the reaction of [$Ru_2(\eta^6$-Arene$)_2Cl_2(\mu$-Cl$)_2$] with the appropriate ligand in (a) methanol at room temperature by adding a large excess of $NaBPh_4$ or (b) methylene chloride with an equimolar quantity of MX (M = Tl or Ag, X^- = BF_4^-, PF_6^-, $CF_3SO_3^-$; M = Na, X^- = $BARF^-$).[15]

When R ≠ H, the two *anti* or *syn* isomers illustrated in Scheme 1, derived from the relative orientation of *ortho*-R-aryl substituents, were observed in solution. The other possible *syn* isomer, having R substituents directed toward the chlorine, never formed. This was probably due to the steric repulsions between R and Cl. The *anti*/*syn* ratio was always close to 2 independent of the counterion nature and solvent utilized in the synthetic procedures. Fractionated crystallizations of the *anti*/*syn* mixtures from methylene chloride/*n*-hexane solutions afforded the pure *anti* isomer when X^- = BPh_4^- or the *syn* isomer when X^- = BF_4^-, PF_6^-, or $CF_3SO_3^-$. Pure *anti* isomers with X^- = BF_4^-, PF_6^-, and $CF_3SO_3^-$ and *syn* isomer with X^- = BPh_4^- were synthesized through anion metathesis using AgX (X^- = BF_4^-, PF_6^-, $CF_3SO_3^-$) in methylene chloride and $NaBPh_4$ salts in methanol, respectively. Solutions of pure *anti* or *syn* isomers were left for several days in all the solvents used. Even at temperatures close to the solvent boiling points there was no appreciable formation of the other isomer.

Intramolecular Characterization in Solution and Conformational Analysis of Cymene Rotation through NOE NMR Experiments. All complexes **1**−**4** were characterized in solution by ^{1}H, ^{13}C, and ^{19}F NMR spectroscopies. Data are reported in the Experimental Section. Numbering of carbon and proton resonances is illustrated in Scheme 1. The higher symmetry of the *syn* isomer makes the two sides of the N,N-ligand, 2/2′ and 3/3′ cymene protons, magnetically equivalent. This reduces the number of observed NMR signals as well as the availability of spatial reporters in the cationic moiety. As a consequence, the results related to the *anti* isomer will have a dominant position in the following descriptions of the arene orientations and relative anion−cation positions.

From ^{1}H, ^{13}C, ^{1}H-COSY, ^{1}H-NOESY, ^{1}H,^{13}C-HMQC NMR, and ^{1}H,^{13}C-HMBC NMR spectroscopies all proton and carbon resonances belonging to the different fragments were easily grouped. On the other hand, the distinction between the resonances of the two sides of the N,N and cymene ligands and the determination of the preferred conformers of cymene were two strictly interlocked and difficult issues. Nevertheless, they were settled as detailed in the following sections.

Complex 3BPh_4 *anti*. As reported in Figure 1, the ^{1}H-NOESY spectrum shows that the intensities of the dipolar interactions between two cymene protons (labeled 2 and 3′ from the intraligand assignment) and 11 or 11′ protons are about twice as high as the analogous ones of the other two cymene protons (2′ and 3). On the contrary, resonances 16 and 16′ (CH_2 protons of Et substituents) show that the dipolar interactions with 2′ and 3 were higher than with 2 and 3′. These observations are consistent with the preferential presence of the two conformers in solution reported in Figure 1, in which the cymene orients the Me and *i*-Pr groups toward the 11′ and 11 protons or *vice versa*, i.e., toward the least hindered regions of space. Since the 11−2 and 11−3′, and 16−3 and 16−2′, NOEs have the same intensities, the two conformers are equally populated.

As far as the distinction between the resonances of the two sides of the N,N ligand is concerned, the ^{1}H-NOESY spectrum shows that the 14−17 dipolar interaction has a significantly higher intensity than the 14′−17′ one (Figure S1). This suggests that 17′ spends less time close to 14′ compared to the time 17 spends close to 14. This is probably due to the ability of 16′ protons to form a weak H-interaction with chlorine. The 17′

(11) For reviews on the application of PGSE NMR to investigate intermolecular interactions: Valentini, M.; Rüegger, H.; Pregosin, P. S. *Helv. Chim. Acta* **2001**, *84*, 2833. Binotti, B.; Macchioni, A.; Zuccaccia, C.; Zuccaccia, D. *Comments Inorg. Chem.* **2002**, *23*, 417. Pregosin, P. S.; Martinez-Viviente, E.; Kumar, P. G. A. *Dalton Trans.* **2003**, 4007. Bagno, A.; Rastrelli, F.; Saielli, G. *Prog. Nucl. Magn. Reson. Spectrosc.* **2005**, *47*, 41. Brand, T.; Cabrita, E. J.; Berger, S. *Prog. Nucl. Magn. Reson. Spectrosc.* **2005**, *46*, 159. Cohen, Y.; Avram, L.; Frish, L. *Angew. Chem., Int. Ed.* **2005**, *44*, 520−554. Pregosin, P. S.; Kumar, P. G. A.; Fernández, I. *Chem. Rev.* **2005**, *105*, 2977. Pregosin, P. S. *Prog. Nucl. Magn. Reson. Spectrosc.* **2006**, *49*, 261.

(12) Gruet, K.; Clot, E.; Eisenstein, O.; Lee, D. H.; Patel, B.; Macchioni, A.; Crabtree, R. H. *New J. Chem.* **2003**, *27*, 80. Appelhans, L. N.; Zuccaccia, D.; Kovacevic, A.; Chianese, A. R.; Miecznikowski, J. R.; Macchioni, A.; Clot, E.; Eisenstein, O.; Crabtree, R. H. *J. Am. Chem. Soc.* **2005**, *127*, 16299. Binotti, B.; Carfagna, C.; Zuccaccia, C.; Macchioni, A. *Chem. Commun.* **2005**, 92−94. Binotti, B.; Bellachioma, G.; Cardaci, G.; Carfagna, C.; Zuccaccia, C.; Macchioni, A. *Chem.−Eur. J.* **2007**, *13*, 1570.

(13) Martinez-Viviente, E.; Pregosin, P. S. *Inorg. Chem.* **2003**, *42*, 2209. Algarra, A. G.; Basallote, M. G.; Fernandez-Trujillo, M. J.; Llusar, R.; Safont, V. S.; Vicent, C. *Inorg. Chem.* **2006**, *45*, 5774.

(14) Preliminary results were previously reported: Zuccaccia D.; Sabatini S.; Bellachioma G.; Cardaci G.; Clot, E.; Macchioni A. *Inorg. Chem.* **2003**, *42*, 5465.

(15) Tom Dieck, H.; Kollvitz, W.; Kleinwachter, I. *Organometallics* **1986**, *5*, 1449.

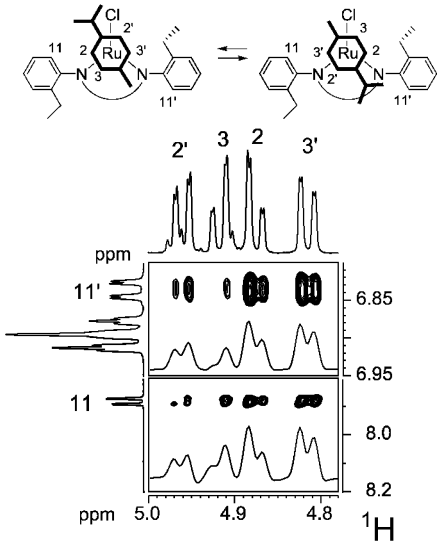

Figure 1. Two sections of the ^{1}H-NOESY NMR spectrum (400.13 MHz, 296 K, methylene chloride-d_2) of the complex **3**BPh$_4$ *anti*. The F2 traces (direct dimension) relative to the 11 and 11′ resonances are reported at the bottom.

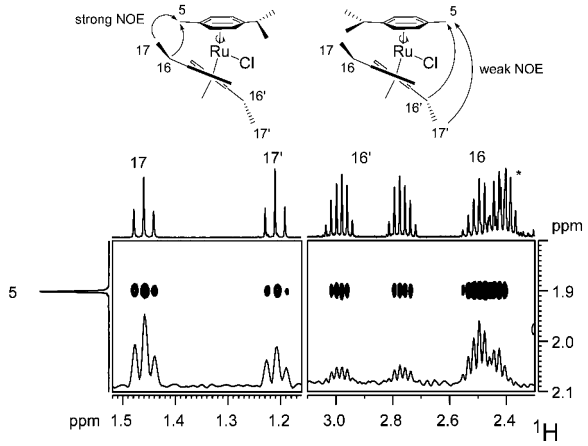

Figure 2. Two sections of the ^{1}H-NOESY NMR spectrum (400.13 MHz, 296 K, methylene chloride-d_2) of the complex **3**BPh$_4$ *anti*. The F2 trace (direct dimension) relative to the 5 resonance is reported at the bottom. * denotes the multiplet of proton 6 superimposed with that of 16.

methyl group is forced to orient far away from the plane that contains N,N,Cl atoms, and the steric repulsion minimization leads to the selection of the orientation where 17′ is more distant from cymene as reported in Figure 2. The latter feeble criterion for distinguishing R from R′ (based on the differential 14/17 and 14′/17′ NOE intensities) is *strengthened* by the observations that both 16 and 17 protons afford appreciably stronger NOEs with 5 cymene protons than do the 16′ and 17′ protons (Figure 2).

4BPh$_4$ *anti* Complex. The dipolar interactions of 2 and 3′ with 11 or 11′ are more intense for this complex than the analogous ones of the other two cymene protons 2′ and 3. Different from **3**BPh$_4$ *anti*, the intensities of the 2′−17′ and 3−17 NOEs are twice as great as those of 2′−17 and 3−17′ (Figure 3). This indicates that the staggered conformation with the *i*-Pr group oriented toward the 11 proton is more populated than the other (Figure 3).

Once the preferential cymene conformer in solution is known, the two R substituents can be easily distinguished. In fact, the 17 methyl group that shows the strongest NOE with the 5 Me group has to be the one directed far away from chlorine (Figure S2). Interestingly, 17′ also interacts dipolarly with 5 but with an intensity about 4 times less than 17.

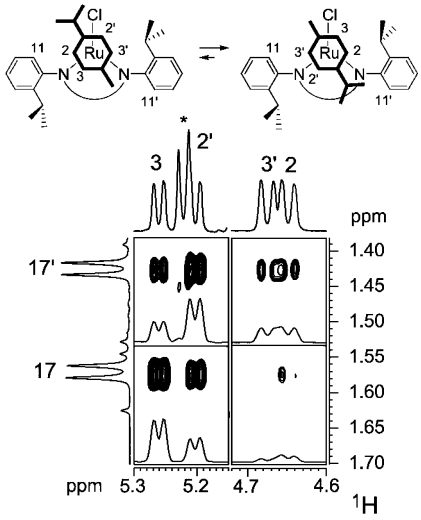

Figure 3. Four sections of the ^{1}H-NOESY NMR spectrum (400.13 MHz, 296 K, methylene chloride-d_2) of the complex **4**BPh$_4$ *anti*. The F2 traces (direct dimension) relative to the 17′ and 17 resonances are reported at the bottom. * denotes the resonance of a small amount of [Ru$_2$(η^6-*p*-cymene)$_2$(μ-Cl$_3$)]BPh$_4$.

2-4BPh$_4$ *syn* Complexes. Only weak dipolar interactions between the protons of R substituents and 5 and isopropyl protons of cymene are observed in the ^{1}H-NOESY NMR spectra; in contrast, 2 and 3 protons show strong NOEs of comparable intensities with R protons. This suggests that cymene orients the alkylic groups almost parallel to the N arms in order to avoid steric interactions with the R substituents.

NMR Interionic Structure in Solution. (a) PGSE Measurements. ^{1}H and ^{19}F-PGSE NMR experiments were carried out for complexes **1**X and **3**X in different solvents, with a relative permittivity (ϵ_r) ranging from 2.27 (benzene-d_6) to 32.66 (methanol-d_4), using tetrakis(trimethylsilyl)silane (TMSS) as internal standard. PGSE measurements allow the translational self-diffusion coefficients (D_t) for both cationic (D_t^+) and anionic (D_t^-) moieties to be determined (Table 1). From the measured self-diffusion coefficients (D_t), the average hydrodynamic radius (r_H) of the diffusing particles were derived by taking advantage of the Stokes−Einstein equation, eq 1:

$$D_t = \frac{kT}{c\pi\eta r_H} \quad (1)$$

where k is the Boltzman constant, T is the temperature, c is a numerical factor, and η is the solution viscosity (Table 1). D_t data were treated by taking all the methodological precautions described in our recent paper.[6] From the average hydrodynamic radii of the aggregates, assumed to be spherical, their volumes (V_H^+ and V_H^-) were obtained.

In order to evaluate the average level of aggregation in solution, V_H^+ and V_H^- can be contrasted with the hydrodynamic volume of ion pairs (V_H^{IP}). We have previously shown that in some cases[5,16] the van der Waals volume (V_{VdW}) of ion pairs, known from the solid state or from calculations, is a good descriptor of V_H^{IP}, while in other cases, it underestimates V_H^{IP}.

(16) Ciancaleoni, G.; Di Maio, I.; Zuccaccia, D.; Macchioni, A. *Organometallics* **2007**, *26*, 489. Claudio Pettinari, C.; Pettinari, R.; Marchetti, F.; Macchioni, A.; Zuccaccia, D.; Skelton, B. W.; White, A. H. *Inorg. Chem.* **2007**, *46*, 896.

Table 1. Diffusion Coefficients ($10^{10}D_t$ m^2 s^{-1}), Hydrodynamic Radius (r_H, Å), *c* Factor, Hydrodynamic Volume (V_H, Å^3), and Aggregation Number (*N*) for Compounds 1 and 3 as a Function of Solvent and Concentration (*C*, mM)

		D_t^+	D_t^-	r_H^+	c^+	r_H^-	c^-	V^+	V^-	N^+	N^-	*C*
					1BF_4 ($V_H^0 = 546$)							
1	chloroform-*d*	7.38	7.41	5.66	5.3	5.63	5.3	759	747	1.4	1.4	30.6
2	chloroform-*d*	6.40	6.76	5.93	5.4	5.68	5.3	873	767	1.6	1.4	50.0
3	CD_2Cl_2	10.8	13.5	5.12	5.3	4.30	5.1	567	333	1.0	0.6	0.08
4	CD_2Cl_2	10.2	11.1	5.22	5.4	4.93	5.3	595	501	1.1	0.9	1.0
5	CD_2Cl_2	10.1	10.8	5.34	5.4	5.04	5.3	637	536	1.2	1.0	1.3
6	CD_2Cl_2	9.8	10.2	5.36	5.4	5.17	5.3	645	578	1.2	1.1	10.0
7	acetone-d_6	12.9	24.0	5.47	5.3	3.48	4.5	685	176	1.3	0.3	5.0
					1PF_6 ($V_H^0 = 566$)							
8	benzene-d_6	6.89	6.82	5.28	5.2	5.32	5.2	613	630	1.1	1.1	0.13
9	benzene-d_6	6.41	6.46	5.48	5.3	5.46	5.3	690	681	1.2	1.2	5.0
10	benzene-d_6	5.19	5.45	6.12	5.4	5.88	5.4	959	851	1.7	1.5	38
11	benzene-d_6	4.24	4.28	6.52	5.5	6.48	5.5	1160	1139	2.1	2.0	85
12	CD_2Cl_2	10.4	11.6	5.13	5.3	4.72	5.2	565	440	1.0	0.8	0.12
13	CD_2Cl_2	9.96	10.9	5.36	5.4	5.00	5.3	645	523	1.1	0.9	3.0
14	acetone-d_6	14.0	28.0	5.11	5.2	3.17	4.2	559	133	1.0	0.2	0.019
15	acetone-d_6	13.3	21.0	5.26	5.3	3.14	4.3	610	130	1.1	0.2	0.45
16	acetone-d_6	12.1	21.0	5.55	5.4	3.7	4.6	716	210	1.3	0.4	18
17	acetone-d_6	10.9	17.8	5.62	5.4	3.79	4.7	744	228	1.3	0.4	62
18	chloroform-*d*	6.98	7.54	5.93	5.4	5.56	5.3	873	720	1.5	1.3	30.1
19	methanol-d_4	7.57	14.8	5.05	5.1	3.20	4.1	540	137	1.0	0.2	2.6
					1BPh_4 ($V_H^0 = 936$)							
20	chloroform-*d*	6.11	6.08	6.72	5.5	6.68	5.5	1271	1248	1.4	1.3	1.6
21	chloroform-*d*	5.96	6.09	6.80	5.5	6.67	5.5	1317	1237	1.4	1.3	7.8
22	CD_2Cl_2	10.8	10.5	5.035.21 (5.21	5.3	5.13	5.3	533	565	0.6	0.6	0.012
23	CD_2Cl_2	9.79	10.0	5.49	5.4	5.40	5.4	693	659	0.7	0.7	0.29
24	CD_2Cl_2	9.14	9.28	5.75	5.5	5.68	5.5	792	767	0.9	0.8	1.8
25	CD_2Cl_2	8.46	8.56	5.92	5.5	5.88	5.5	869	851	0.9	0.9	13.3
26	CD_2Cl_2	7.85	7.95	5.94	5.5	5.89	5.5	877	855	0.9	0.9	40.0
27	CD_2Cl_2	7.62	7.74	6.00	5.5	5.94	5.5	904	877	1.0	0.9	47.5
28	acetone-d_6	13.3	15.7	5.33	5.3	4.69	5.1	634	432	0.7	0.5	0.2
29	acetone-d_6	12.6	14.3	5.55	5.4	4.99	5.2	716	520	0.8	0.6	2.0
30	acetone-d_6	12.0	13.8	5.62	5.4	5.04	5.2	743	536	0.8	0.6	8
31	acetone-d_6	11.1	12.7	5.77	5.4	5.23	5.2	804	599	0.9	0.6	31
					1BARF ($V_H^0 = 1313$)							
32	CD_2Cl_2	11.8	8.90	4.94	5.3	6.03	5.5	504	918	0.4	0.7	0.004
33	CD_2Cl_2	9.56	8.33	5.47	5.4	6.14	5.5	685	969	0.5	0.7	1.0
34	CD_2Cl_2	8.39	7.45	5.95	5.5	6.53	5.6	882	1166	0.7	0.9	32.0
35	2-propanol-d_8	1.66	1.44	5.5	5.0	6.1	5.2	700	969	0.5	0.7	30.1
36	acetone-d_6	12.2	11.7	5.56	5.3	5.78	5.4	623	809	0.5	0.6	0.17
37	acetone-d_6	12.8	12.0	5.46	5.4	5.79	5.4	681	813	0.5	0.6	2.1
38	benzene-d_6	3.7414	3.72	8.82	5.7	8.78	5.7	2835	2874	2.1	2.1	5.1
					3BF_4 *anti* ($V_H^0 = 616$)							
39	benzene-d_6	5.14	5.15	6.50	5.5	6.49	5.5	1150	1145	1.9	1.9	34.1
40	chloroform-*d*	6.73	7.15	6.00	5.3	5.71	5.3	904	775	1.5	1.3	34.0
41	CD_2Cl_2	8.86	9.94	5.66	5.5	5.16	5.4	759	575	1.2	0.9	34.1
42	2-propanol-d_8	2.01	2.65	5.26	4.9	4.36	4.5	609	346	1.0	0.6	0.2
43	2-propanol-d_8	1.94	2.34	5.40	5.0	4.72	4.7	659	440	1.1	0.7	3.2
44	2-propanol-d_8	1.84	2.06	5.60	5.1	5.17	4.9	735	578	1.2	0.9	19.8
45	2-propanol-d_8	1.75	1.94	5.84	5.1	5.41	5.1	833	662	1.4	1.1	39.6[a]
46	acetone-d_6	11.8	19.5	5.83	5.3	3.89	4.8	830	246	1.4	0.4	34.1
47	ethanol-d_6	3.80	4.63	5.35	5.0	4.66	4.7	641	423	1.0	0.7	34.1
48	methanol-d_4	7.08	11.1	5.29	5.2	3.84	4.5	620	237	1.0	0.4	34.0
					3BPh_4 *anti* ($V_H^0 = 1006$)							
49	benzene-d_6	5.87	6.00	6.56	5.5	6.46	5.5	1182	1129	1.2	1.1	0.4[a]
50	chloroform-*d*	4.90	4.85	7.64	5.7	7.68	5.7	1867	1897	1.9	1.9	31.0
51	CD_2Cl_2	7.83	8.03	6.13	5.6	6.02	5.5	964	913	1.0	0.9	43.0
52	acetone-d_6	10.8	12.6	5.80	5.5	5.12	5.3	817	562	0.8	0.6	31.8
					3CF_3SO_3 *anti* ($V_H^0 = 646$)							
53	chloroform-*d*	6.17	6.41	6.33	5.5	6.12	5.5	1062	960	1.6	1.5	31.3
54	2-propanol-d_8	1.74	1.94	5.49	5.1	5.14	5.0	693	568	1.1	0.9	31.0
55	methanol-d_4	7.08	10.6	5.28	5.1	3.98	4.6	616	264	1.0	0.4	31.5

[a] Saturated solution.

A much more reliable procedure for evaluating the level of aggregation is based on comparing V_H with the hydrodynamic volume at the lowest concentration value (V_H^0).[17] It seems that V_{VdW} describes V_H^{IP} well only if the molecules are nearly spherical in shape and do not have inlets. One can determine whether V_{VdW} is a good descriptor of V_H^{IP} by measuring V_H^0 through diffusion measurements at low concentration (ca. 10^{-5} M) and/or by using solvents where it is supposed that the molecules are less aggregated. Trends of V_H versus C were determined for **1**BF_4 (Table 1, entries 3−6), **1**BPh_4 (Table 1, entries 22−27), and **1**BARF (Table 1, entries 32−34) in CD_2Cl_2 and for **1**BPh_4 in acetone-d_6 (Table 1, entries 28−31). The lowest measured value for the hydrodynamic volume of $\mathbf{1}^+$ was 504 Å^3 observed in a 0.004 mM solution of **1**BARF in CD_2Cl_2

(Table 1, entry 32). The latter was taken as V_H^0 for $\mathbf{1}^+$. From measurements in acetone-d_6, the V_H^0 for BPh_4^- and $BARF^-$ counterions were determined to be 432 (Table 1, entry 28) and 809 Å^3 (Table 1, entry 36), respectively. V_H^0 for small counterions was considered equal to V_{VdW} (62 Å^3 for PF_6^-, 42 Å^3 for BF_4^-, and 72 Å^3 for $CF_3SO_3^-$). V_H^0 of **1**X ion pairs was derived by adding the volumes of the single ions (Table 1). It can be seen that the determined V_H^0 of $\mathbf{1}^+$ is ca. 1.35 times higher than V_{VdW} (372 Å^3). Since $\mathbf{3}^+$ has a shape similar to that of $\mathbf{1}^+$, its V_H^0 (574 Å^3) was derived by scaling V_{VdW} (424 Å^3) by the same factor (1.35). V_H^0 of **3**X ion pairs was obtained by adding the volume of the counterion to V_H^0 of $\mathbf{3}^+$ (Table 1).

The ratios (N^+ and N^-, respectively) between the hydrodynamic volume (V_H^+ and V_H^-, respectively) and V_H^0 for the ion pairs are reported in Table 1. They represent a sort of aggregation number.[18] Since a distribution of ionic species is present in solution, the N^+ or N^- indicates the apparent average aggregation number of the ionic moieties. For example, if both of them are equal to 1 or 2, this means that ion pairs or ion quadruples, i.e., "$(Ru^+X^-)_2$", are the predominant species in solution, respectively. The interpretation of the N values is less intuitive when there is a significant presence of odd aggregates in solution, i.e., when $N < 1$ or $N^+ \neq N^-$, due to the different volumes of the single ionic fragments. In such cases, N values can be discussed considering the volumes of the free ions. Theoretical N values for the free ions in our complexes are as follows: $N^+ = 0.92$ and $N^- = 0.08$ for **1**BF_4, $N^+ = 0.89$ and $N^- = 0.11$ for **1**PF_6, $N^+ = 0.54$ and $N^- = 0.46$ for **1**BPh_4, $N^+ = 0.38$ and $N^- = 0.62$ for **1**BARF, $N^+ = 0.93$ and $N^- = 0.07$ for **3**BF_4 *anti*, $N^+ = 0.57$ and $N^- = 0.43$ for **3**BPh_4 *anti*, and $N^+ = 0.89$ and $N^- = 0.11$ for **3**CF_3SO_3 *anti*. If N^+ and/or N^- in Table 1 are larger than the previously indicated aggregation number, then ion pairing and/or aggregation occurs. It should be noted that the N values reported in Table 1 are lower than those reported earlier[14] because, in that case, they were calculated by the ratio of V_H and V_{VdW}.

All of the measurements indicated a certain level of aggregation that was found to be quite insensitive to the size of the *ortho*-R groups (compare entries 1 with 40 or 26 with 51 in Table 1). The level of aggregation was, however, affected by the choice of the solvent, counterion, and concentration.

Solvent Effect on Aggregation. The tendency to aggregate for all complexes decreases as ϵ_r increases. In solvents that have a ϵ_r higher than that of chloroform-*d*, N^+ and N^- are very often less than 1 and, consequently, free ions and ion pairs are the predominant species. In chloroform-*d* (Table 1, entries 1−2, 18, 20−21, 40, 50, and 53) and benzene-d_6 (Table 1, entries 8−11, 38, 39, and 49), N^+ and N^- assume the same values that significantly exceed 1, which clearly indicates that ion pairs associate forming ion quadruples. In 2-propanol-d_8 and acetone-d_6, having an intermediate values of ϵ_r, the complexes with small counterions show N^+ values that are slightly greater than 1 (Table 1, entries 7, 14−17, 42−45, 54), while the N^- values are less than 1. It is difficult to say if this is due to a partial formation of "Ru_2X^+" ion triples or to the hydrodynamic properties of such solvents. Perhaps, the most important finding concerning the effect of solvent on aggregation is that, when ϵ_r is kept constant, the aggregation tendency increases in protic solvents. This is clearly shown in Figure 4, where N^+ and N^- for complex **3**BF_4 *anti* as a function of ϵ_r are reported. The N^+ values are identical (Table 1, entries 45 and 46), but the N^- values are 1.1 and 0.4 in 2-propanol-d_8 and acetone-d_6, respectively, while the ϵ_r values are almost the same.

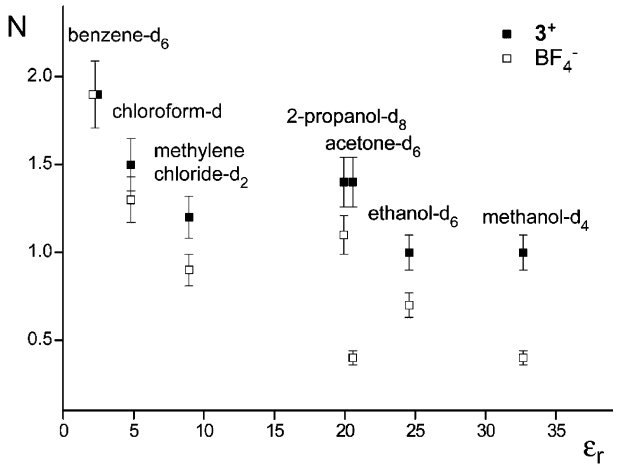

Figure 4. Aggregation number for the cation (N^+) and anion (N^-) of complex **3**BF_4 *anti* as a function of the solvent relative permittivity (ϵ_r).

Counterion Effect on Aggregation. The results of PGSE NMR measurements performed for complexes **1**X ($X^- = BF_4^-$, PF_6^-, BPh_4^-, and $BARF^-$) in CD_2Cl_2 at similar concentrations are reported in Table 1, entries 5, 13, 24, and 33. They indicate that the ion-pairing tendency follows the order BF_4^- ($N^+ = 1.2$, $N^- = 1.0$) ≈ PF_6^- ($N^+ = 1.1$, $N^- = 0.9$) > BPh_4^- ($N^+ = 0.9$, $N^- = 0.8$) > $BARF^-$ ($N^+ = 0.5$, $N^- = 0.7$). The effect of the counterion on the tendency to form ion quadruples from ion pairs can be deduced from the PGSE results for **3**X *anti* in chloroform-*d* [Table 1, entries 40, 50, and 53; BPh_4^- ($N^+ = 1.9$, $N^- = 1.9$) > $CF_3SO_3^-$ ($N^+ = 1.6$, $N^- = 1.5$) ≈ BF_4^- ($N^+ = 1.5$, $N^- = 1.3$)] and **1**X in benzene-d_6 [Table 1, entries 9 and 38; $BARF^-$ ($N^+ = 2.1$, $N^- = 2.1$) > PF_6^- ($N^+ = 1.2$, $N^- = 1.2$)]. For both complexes the least coordinating counterions favored the formation of ion quadruples.

Concentration Effect on Aggregation. As expected, the aggregation tendency increases with the concentration, but the nature of the counterion and solvent are critical. For instance, complexes with small counterions (BF_4^-, PF_6^-, and $CF_3SO_3^-$) in CD_2Cl_2 afford complete ion pairing already at ca. 1 mM (Table 1, entry 4). In contrast, complex **1**BPh_4 leads to complete ion pairing at ca. 15 mM (Figure 5, Table 1 entries 22−27), while **1**BARF never reaches complete ion pairing even at 32 mM (Table 1, entries 34). As stated before, complete ion pairing is observed in chloroform-*d* and benzene-d_6 even at the lowest investigated concentration. An increase of concentration in such solvents causes the aggregation of ion pairs into ion quadruples. The case of complex **1**PF_6 in benzene-d_6 is reported in Figure 5: complete formation of ion quadruples occurs at ca. 80 mM. A comparison of the concentration trends in acetone-d_6 and 2-propanol-d_8 confirms that the latter has a greater tendency to undergo ion pairing. This can be noted by looking at entries 14−17 and 42−45 in Table 1. While ion pairing is complete in 2-propanol-d_8 at ca. 20 mM (Table 1, entry 44), in acetone-d_6 (Table 1, entry 16) it is only marginal at the same concentration.

(b) NOE Measurements. The relative anion−cation orientations in solution for complexes **1**−**4**X were determined by detecting dipolar interionic interactions in the $^{19}F,^1H$-HOESY

(17) Zuccaccia, D.; Pirondini, L.; Pinalli, R.; Dalcanale, E.; Macchioni, A. *J. Am. Chem. Soc.* **2005**, *127*, 7025. Kang, H.; Facchetti, A.; Zhu, P.; Jiang, H.; Yang, Y.; Cariati, E.; Righetto, S.; Ugo, R.; Zuccaccia, C.; Macchioni, A.; Stern, C. L.; Liu, Z.; Ho, S.-T.; Marks, T. J. *Angew. Chem., Int. Ed.* **2005**, *44*, 7922. Menozzi, E.; Busi, M.; Massera, C.; Ugozzoli, F.; Zuccaccia, D.; Macchioni, A.; Dalcanale, E. *J. Org. Chem.* **2006**, *71*, 2617.

(18) (a) Pochapsky, S. S.; Mo, H.; Pochapsky, T. *J. Chem. Soc., Chem. Commun.* **1995**, 2513. (b) Mo, H.; Pochapsky, T. *J. Phys. Chem. B* **1997**, *101*, 4485. (c) Zuccaccia, C.; Bellachioma, G.; Cardaci, G.; Macchioni, A. *Organometallics* **2000**, *19*, 4663.

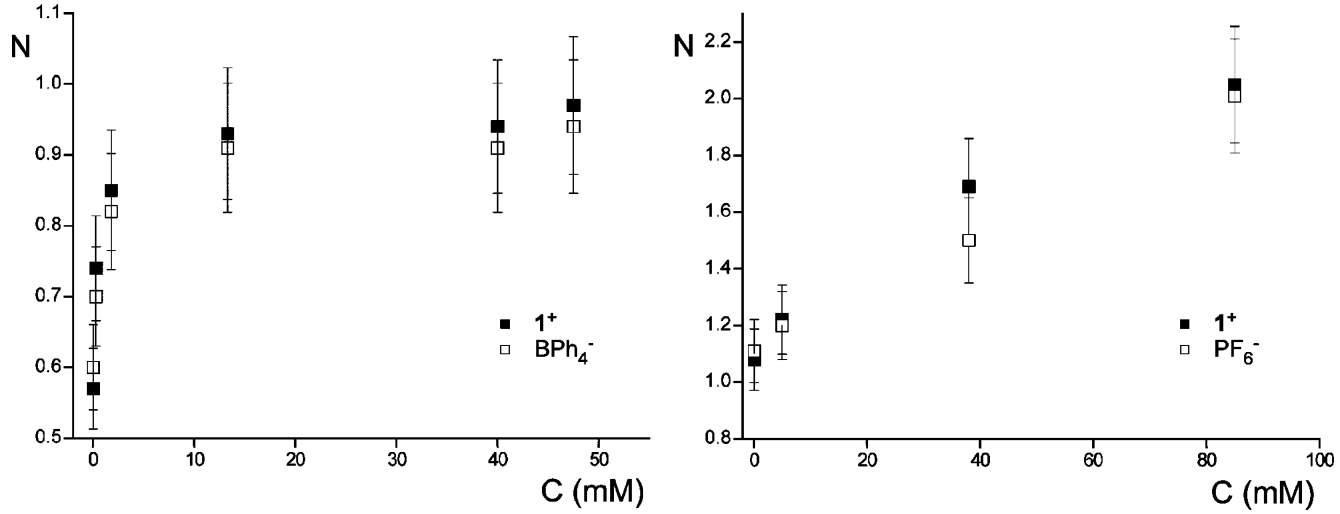

Figure 5. Aggregation number for the cation (N^+) and anion (N^-) of complexes **1**BPh_4 in CD_2Cl_2 (left) and **1**PF_6 in benzene-d_6 (right) as a function of the concentration (C).

($X^- = BF_4^-$, PF_6^-, $CF_3SO_3^-$, $BARF^-$) and ^{1}H-NOESY ($X^- = BPh_4^-$) NMR spectra at room temperature (296 K). The following solvents differing in both relative permittivity (ϵ_r) and nature were taken into account: benzene-d_6 ($\epsilon_r^{25°C} = 2.27$), chloroform-d ($\epsilon_r^{20°C} = 4.81$), methylene chloride-d_2 ($\epsilon_r^{25°C} = 8.93$), isopropanol-d_8 ($\epsilon_r^{25°C} = 19.92$), acetone-$d_6$ ($\epsilon_r^{25°C} = 20.56$), ethanol-$d_6$ ($\epsilon_r^{25°C} = 24.55$), methanol-$d_4$ ($\epsilon_r^{25°C} = 32.66$), nitromethane-$d_3$ ($\epsilon_r^{25°C} = 35.94$), and dimethylsulfoxide-d_6 ($\epsilon_r^{25°C} = 46.45$).

Interionic NOEs were not detected in nitromethane-d_3. In all other cases, anion−cation dipolar interactions were observed with intensities that decreased as ϵ_r increased and, interestingly, were higher for protic solvents when pairs of solvents with similar ϵ_r values were compared. In fact, NOEs were much more intense in isopropanol-d_8 ($\epsilon_r^{25°C} = 19.92$) than in acetone-$d_6$ ($\epsilon_r^{25°C} = 20.56$);[19] they were observed in methanol-d_4 ($\epsilon_r^{25°C} = 32.66$) but were not detected in the almost isodielectric nitromethane-d_3 ($\epsilon_r^{25°C} = 35.94$).[20]

The preferred relative anion−cation orientations that can be deduced from the observed interionic NOEs depend little on the R substituents and solvent, while they are affected greatly by the nature of the counterion. In particular, two different situations were observed for small (BF_4^-, PF_6^-, $CF_3SO_3^-$) and large (BPh_4^-, $BARF^-$) counterions.

Interionic NOEs when $X^- = BF_4^-$, PF_6^-, or $CF_3SO_3^-$. For *anti* compounds, strong contacts were observed between F atoms of the counterion and 8, 8′, 11′, and R resonances. Weak contacts were detected with all cymene resonances and with 12′ and 14, while the anion did not show any interaction with R protons pointing toward the chloride. The only difference for *syn* compounds was the lack of interaction between X^- and 11.

A quantitative analysis of interionic NOE intensities was carried out taking into account that the volumes of the cross-peaks are proportional to ($n_I n_S/n_I + n_S$), where n_I and n_S are the number of equivalent I and S nuclei, respectively.[10,21,22] The main results are reported in Table 2. In particular, two limiting situations were considered for **3**BF_4 *anti* based on the PGSE results: in CD_2Cl_2 where there is a predominance of ion pairs (Table 2, entry 1) and in benzene-d_6 where ion quadruples are predominant (Table 2, entry 2). In the former case, BF_4^- is located above the plane containing the C═N imine moieties and is shifted toward the less hindered N arm having the Et group pointing toward the chlorine atom. Although BF_4^- is confined in such a position by the two aryls of the N,N ligand that are almost perpendicular to the plane bearing the C═N groups, it can still interact weakly with cymene protons. Few changes are observed in NOE intensities on passing from CD_2Cl_2 (ion pairs, entry 1 in Table 2) to benzene-d_6 (ion quadruples, entry 2 in Table 2): NOEs with Et and cymene (all except 7/7′) protons have a higher intensity in ion quadruples than in ion pairs. Having normalized the NOE intensity between F nuclei of the counterion and 8/8′ protons to 1, it is clear that in ion quadruples there is an average shift of the counterions toward cymene. In the *syn* isomer (Table 2, entry 3) the anion is located in a more central position with respect to the N,N ligand that now has equally hindered arms.

Table 2. Relative NOE Intensities Determined by Arbitrarily Fixing the Intensity of the NOE(s) between the Anion Resonances (*o*-H in the case of BPh_4^-) and the Imine Methyls (8 and 8′) at 1

		8/8′	16	17	11′	2/3	7/7′	5
1	**3**BF_4 *anti*[a]	1	1.23	0.46	1.78	0.17	0.10	0.25
2	**3**BF_4 *anti*[b]	1	1.50	0.76	1.68	0.51	0.16	0.58
3	**3**BF_4 *syn*[b]	1	1.42	0.61		0.28	0.13	0.24
4	**3**CF_3SO_3 *anti*[c]	1	0.97	1.38	1.39	0.60	0.46	0.75
5	**3**BPh_4 *anti*[c]	1	0.85	0.54	*d*	1.47	0.38	0.70
6	**3**BPh_4 *anti*[a]	1	0.79	0.49	*d*	1.92	0.44	0.92
7	**3**BPh_4 *syn*[c]	1	1.33	0.72		1.60	0.40	1.11

[a] In CD_2Cl_2 at 286 K. [b]In benzene-d_6 at 296 K. [c]In chloroform-d at 296 K. [d]Difficult to quantitatively evaluate due to the overlapping of cationic and anionic resonances.

Very few differences were observed in the NOE intensities for the various fluorinated anions, which indicates that the latter are located in the same position. One of the few differences was that while BF_4^- showed a stronger interaction with CH_2 than with CH_3 of the Et′ substituent in **3** *anti* (Table 2, entry 1), the contrary was observed with $CF_3SO_3^-$ (Table 2, entry 4). This is not necessarily due to a variation in the position of the anion. It can be explained by considering that while the head of the triflate anion (SO_3) is located in the same position

(19) Evans, D. F.; Gardam, P. *J. Phys. Chem.* **1968**, *72*, 3281. Evans, D. F.; Thomas, J.; Nadas, J. A.; Matesich, M. A. *J. Phys. Chem.* **1971**, *75*, 1714.
(20) Miller, R. C.; Fuoss, R. M. *J. Phys. Chem.* **1953**, *75*, 3076.
(21) Macchioni, A.; Magistrato, A.; Orabona, I.; Ruffo, F.; Röthlisberger, U.; Zuccaccia, C. *New J. Chem.* **2003**, *27*, 455.
(22) Macura, S.; Ernst, R. R. *Mol. Phys.* **1980**, *41*, 95.

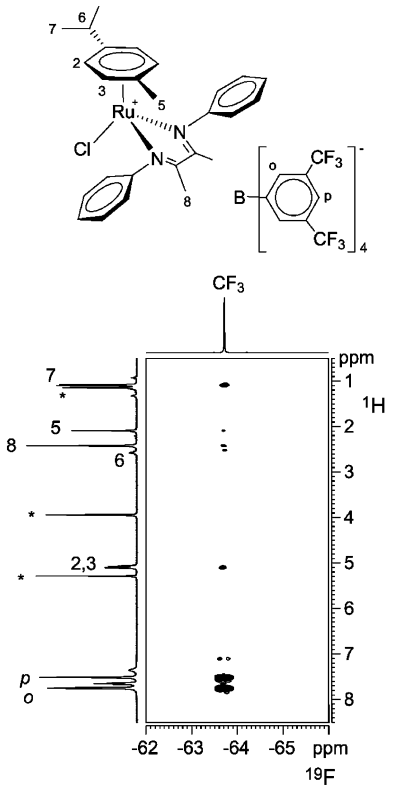

Figure 6. $^{19}F,^{1}H$-HOESY NMR spectrum (376.65 MHz, 296 K, 2-propanol-d_8) of complex **1**BARF. * denote the residues of nondeuterated solvent.

as BF_4^-, its tail (CF_3) is pointed far away from the α-diimine carbon plane toward the methyl group of the R substituent.

Interionic NOEs When X^- = BPh_4^- or $BARF^-$. These anions afforded much stronger NOEs with cymene protons, as can be seen from Table 2 (entries 5−7). The intensities of the interionic NOEs with cymene protons are comparable or even higher than those with 8, 8′, 11′, or Et. The quantitative analysis of NOE intensities does not allow finding a single anion−cation orientation that explains the data. However, there must be a certain level of specific interactions because these large counteranions do not show any NOE with the R group pointing toward the chlorine in the *anti* isomers. It is remarkable that interionic NOEs were clearly observed in the $^{19}F,^{1}H$-HOESY spectrum of **1**BARF in isopropanol-d_8 (Figure 6), since $BARF^-$ is considered as one of the weakest coordinating counterions and is being used with greater frequency in organometallic chemistry and homogeneous catalysis.

X-ray Studies. Intramolecular Results. The solid-state structures of compounds **1**BPh_4, **2**BF_4 *syn*, **3**BPh_4 *anti*, **4**BPh_4 *anti*, and **5**PF_6 were determined through single-crystal X-ray diffractometric investigation. All five complexes exhibit a three-legged piano stool pseudo-octahedral geometry where the arene occupies three adjacent sites of the octahedron. Intramolecular bond lengths and angles fall in the typical ranges observed for analogous compounds and will be discussed only briefly here.[23] As an example of the geometrical features, two ORTEP views of **4**BPh_4 *anti* and **2**BF_4 *syn* cations are reported in Figure 7.

Cymene and 2-monosubstituted aryl moieties of the diimine ligand are roughly coplanar, with angles between the two planes ranging from 159.0° to 173.3° and from 156.9° to 173.0° for N′- and N-aryl substituents, respectively. The latter form an angle with the RuNN′ plane that ranges from 49.2° to 80.5°. Cymene orientation was evaluated by measuring the C1−cymene centroid−Ru−Cl torsion angle considering clockwise angles with a positive sign: **1**BPh_4, 31.7°; **2**BF_4 *syn*, 72.3°; **3**BPh_4 *anti*, 12.2°; and **4**BPh_4 *anti*, −11.2°. Compound **1**BPh_4 exhibits an almost ideal staggered orientation of cymene with a torsion angle that approaches 30°; the isopropyl group of cymene is directed between the N and N′ arms. In **3**BPh_4 *anti* and **4**BPh_4 *anti* an intermediate situation between staggered and eclipsed cymene orientation is reached, probably due to the increased steric interactions. The isopropyl group of cymene is directed between the N and N′ arms, as in **1**BPh_4. A completely different situation occurs in **2**BF_4 *syn*: the isopropyl and methyl cymene groups are oriented along the N,N-axis due to the steric hindrance introduced by the *ortho* diimine substituents that are both pointed toward the cymene.

Interionic Structure. Analogous to what is observed in solution, the solid-state interionic structure is also strongly affected by the nature of the anion. Some common features can be found in the interionic structures of **1**BPh_4, **3**BPh_4 *anti*, and **4**BPh_4 *anti*. Each cation is surrounded by two anions (Figure 8). One is positioned on the side of the cymene ligand and orients a phenyl ring almost coplanarly with the cymene ring to give $\pi-\pi$ stacking interactions (A in Figure 8, left). The angle between the two rings is 11.2° (**1**BPh_4), 16.1° (**3**BPh_4 *anti*), and 27.2° (**4**BPh_4 *anti*), while the mean slip angle between the normal of the cymene plane and the centroid vector of the phenyl ring is 28.4° (**1**BPh_4), 11.3° (**3**BPh_4 *anti*), and 12.8° (**4**BPh_4 *anti*), and the centroid to centroid distance is 3.94 (**1**BPh_4), 3.87 (**3**BPh_4 *anti*), and 4.08 Å (**4**BPh_4 *anti*). In addition, there is a CH$-\pi$ interaction between one hydrogen atom of the cymene ring and another phenyl group of the anion. The other anion is positioned on the side of the N,N ligand and shows contacts between the three hydrogen atoms of the imine methyls and the phenyl group (B in Figure 8, left). No significant intercationic interactions are present. Consequently, there is an alternation of cations and anions, with the latter bridging two differently oriented cations.

In complex **2**BF_4 *syn* the cation is surrounded by four anions (A, B, C, and D in Figure 8, right). Two of them are much closer than the others (A, Ru−B 5.80 Å, and B, Ru−B 6.05 Å, in Figure 8, right). One is adjacent to the cymene group on the opposite side of the Cl (A in Figure 8, bottom). The fluorine atoms of the anion moiety show interactions as short as 2.50 Å with cymene hydrogen atoms. The other anion is located above the N═C−C═N moiety (B in Figure 8, right) and shows several short F···H contacts.

In complex **5**PF_6 the closest anion is located as B in complex **2**BF_4 *syn*. Since no alkyl substituents are present in the aryl rings, the counterion can approach the cation closely:[24] the Ru−P distance is equal to 5.23 Å, which is considerably shorter than in **2**BF_4 *syn* (Ru−B 6.05 Å).

While an alternation of cations and anions is observed in the solid state for **1**BPh_4, **3**BPh_4 *anti*, and **4**BPh_4 *anti*, **2**BF_4 *syn* and **5**PF_6 show anion/cation, cation/cation, and anion/anion proximities. Figure 9 shows the different types of ion quadruples that are present in the solid-state structures of **2**BF_4 *syn* and **5**PF_6.

(23) CCDC 634218−634222 contain the supplementary crystallographic data for this paper. These data can be obtained free of charge from the Cambridge Crystallographic Data Centre via www.ccdc.cam.ac.uk/data_request/cif/.

(24) Zuccaccia, C.; Macchioni, A.; Orabona, I.; Ruffo, F. *Organometallics* **1999**, *18*, 4367. Bellachioma, G.; Binotti, B.; Cardaci, G.; Carfagna, C.; Macchioni, A.; Sabatini, S.; Zuccaccia, C. *Inorg. Chim. Acta* **2002**, *350*, 44. Binotti, B.; Carfagna, C.; Foresti, E.; Macchioni, A.; Sabatino, P.; Zuccaccia, C.; Zuccaccia, D. *J. Organomet. Chem.* **2004**, *689*, 647.

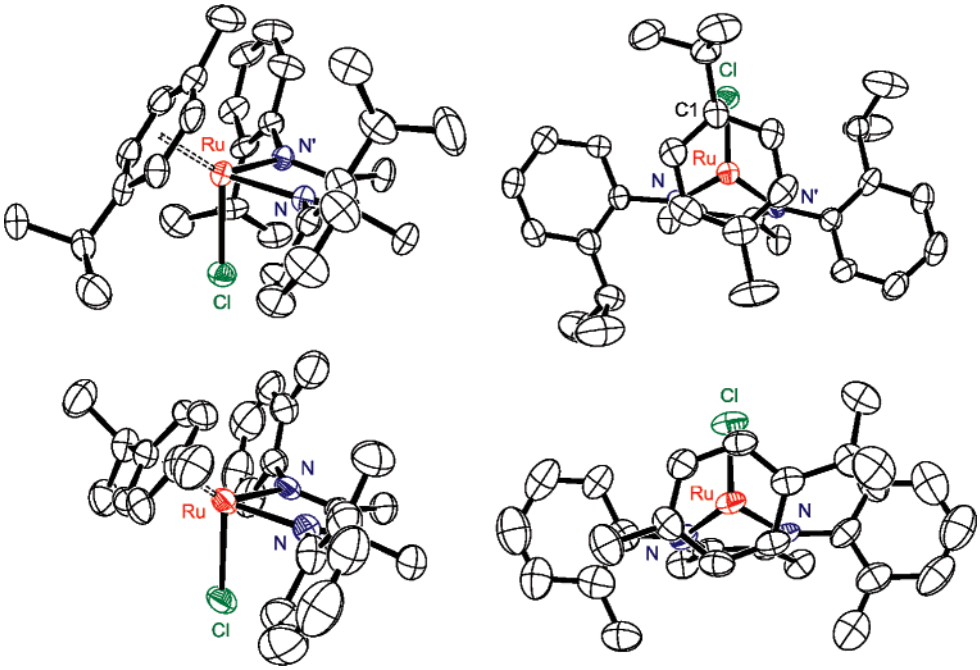

Figure 7. Two ORTEP (30% ellipsoid probability) views of $\mathbf{4}^+$ *anti* (top) and $\mathbf{2}^+$ *syn* (bottom) showing the different cymene orientations.

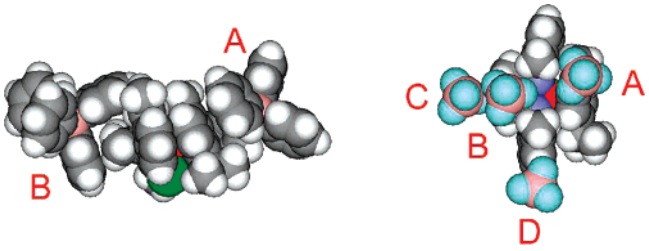

Figure 8. Anion orientations observed for **3**BPh_4 *anti* (left) and **2**BF_4 *syn* (bottom, right) in the solid state.

In the two top structures in Figure 9, two counterions bridge the cationic units; intercationic interactions are present in the remaining ones. Interestingly, two cooperative intercationic Ru−Cl···H (of cymene moiety) interactions (2.81 Å) are present in **2**BF_4 *syn* (Figure 9, bottom left) with a Ru···Ru distance equal to 6.84 Å. The closest intercationic contacts in **5**PF_6 occur between Cl and H protons of diimine Me groups (Cl···H 2.79 Å) with a Ru···Ru distance equal to 7.46 Å.

Theoretical Calculations. Geometry and Conformers of $\mathbf{3}^+$. *Syn* and *anti* isomers of cation $\mathbf{3}^+$ were optimized at the B3PW91 level (see Computational Details). In each case, three orientations of the cymene ring were considered: Me toward Cl (**3anti_00**, **3syn_00**), Me opposite Cl (**3anti_180**, **3syn_180**), and cymene substituents along the N−N axis (**3anti_90**, **3syn_90**). Figure 10 shows the corresponding geometries with hydrogen atoms omitted for clarity (selected geometrical parameters are reported in the Supporting Information). The *syn* isomer with both ethyl chains toward the Cl is not searched, as it was not seen experimentally; it is thought to be at high energy due to steric repulsions between the ethyl groups and Cl.

The geometries of all the isomers are very similar and can be described as that of a piano stool with cymene as the stool and the two diimine N atoms and Cl as the legs. The torsional angle δ = Cl−Ru−D1−C5 describes the orientation of cymene with respect to the plane bisecting the diimine ligand (D1 is the centroid of the cymene benzene ring) and is independent of the presence of one (*anti*) or two (*syn*) ethyl chains on the same side. When the Me group points away from the Cl, δ is close to 180° (**3anti_180**, δ = 171.3°; **3syn_180**, δ = 172.5°). For the *anti* isomer, the Me and *i*-Pr groups are slightly displaced in the quadrants where no ethyl chain is present (Figure 10). When Me points toward the Cl, the cymene is less symmetrically positioned with δ amounting to ca. 25° in a staggered-like conformation (**3anti_00**, δ = 24.4°; **3syn_00**, δ = 25.8°). Interestingly, in the *anti* isomer, the preferred conformation is that with both cymene substituents close to the ethyl chains. Attempts to locate the other conformer with Me and *i*-Pr in the less bulky quadrants failed, as **3anti_00** was always recovered.

The piano stool geometry introduces a dissymmetry in the orientation of the cymene ring plane with respect to the five-membered ring defined by Ru and the diimine ligand, as illustrated by the values of the Ru−D1−C5 and D1−Ru−D2 angles (Table S1, D2 is the centroid of the five-membered Ru−N−C−C−N ring). Consequently, for the phenyl rings on the diimine ligands, the side opposite the Cl is closer to the cymene ring. In **3anti_180**, the shortest contact H5···H16 with the ethyl chain is 2.48 Å. This value is significantly shorter than H5···H16 in **3anti_00** (3.142 Å) when Me points toward the Cl. This is in agreement with the experimental observations of a strong NOE in the former case and a weak one in the latter (Figure 2).

The ethyl chain on the Cl side has a different conformation than the one on the other side in the *anti* isomers. In the latter, the ethyl chain lies slightly above the phenyl ring toward the cymene (22.7°, **3anti_00**; 17.7°, **3anti_180**), whereas the ethyl chain toward the Cl is perpendicular to the phenyl ring (98.8°, **3anti_00**; 93°, **3anti_180**). This orientation is due to a stabilizing interaction that develops between one methylene proton and the Cl atom, as illustrated by short H···Cl contacts (2.488 Å, **3anti_00**; 2.513 Å, **3anti_180**), and to a minimization of the steric repulsion.

There are also several short H···H contacts that can be used to rationalize the NOE observations. For **3anti_180**, the short contact 3.23 Å is between H2 and H11′, together with the contacts between H5 and both H11 (2.56 Å) and H16 (2.48 Å). The H3···H11 contact is longer (3.678 Å). For **3anti_00**, there are shorter contacts with H11 for H2 (2.854 Å) and H3 (3.022

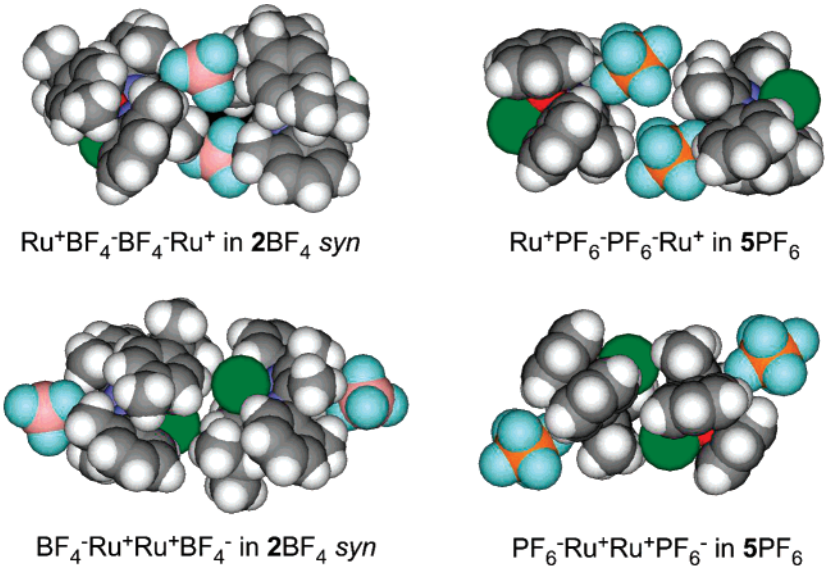

Figure 9. Ion quadruples observed in the solid state for $2BF_4$ *syn* and $5PF_6$.

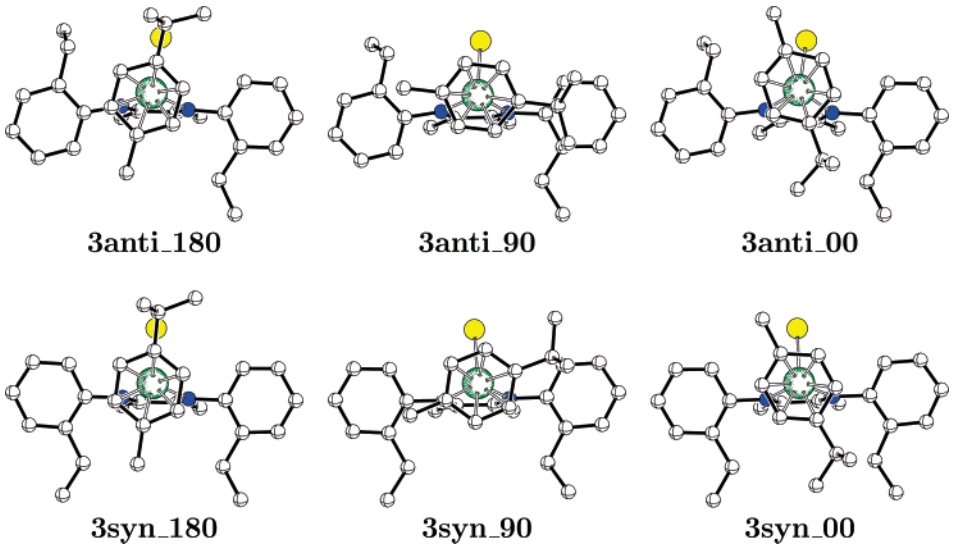

Figure 10. Optimized geometries of the various conformers for 3^+ *anti* and *syn*. Hydrogen atoms are omitted for clarity.

Table 3. Electronic Energy (*E*), Corrected Zero-Point Energy (*E*+ZPE), and Gibbs Free Energy (*G*) Values (kJ mol^{-1}) for the Different Conformers of 3^+ Optimized at the B3PW91 Level

	3anti_00	3anti_90	3anti_180	3syn_00	3syn_90	3syn_180
E	3.8	22.7	0.0	0.3	4.2	−3.5
E+ZPE	3.9	22.9	0.0	0.6	3.9	−3.9
G	4.4	29.0	0.0	0.5	4.0	−5.2

Å), in agreement with the larger NOE intensities that were observed experimentally (Figure 1).

Table 3 displays the relative energies of the various complexes with **3anti_180** as a reference. Since no significant differences are observed if the zero-point energy correction is included or if the Gibbs free energy values are considered, only the electronic energy values, *E*, are discussed. Contrary to what is observed experimentally, the *syn* isomer, **3syn_180**, is calculated to be more stable than the *anti* isomer, **3anti_180**, albeit by only 3.5 kJ mol^{-1}. All the isomers have very similar energies, and from the calculations there is no strongly preferred conformer. The close energy values of the conformers with $\delta = 90°$ (**3anti_90** and **3syn_90**) support a very easy cymene rotation, as observed in NMR. This is also in agreement with the observation of two conformers for 3^+ *anti* as shown in Figure 10; the calculated energy difference between **3anti_00** and **3anti_180** is very small (3.8 kJ mol^{-1}). The energy values are also in agreement with the different orientations of the cymene ring observed in the X-ray structures (3^+ *anti* and 2^+ *syn*); the actual orientation of cymene is not an energetically costly process, and crystal packing forces may easily overcome preferred orientations.

Anion-Dependent Ion Pair Structures. In order to gain some insight into the structure and energetics of the ion pairs, ONIOM calculations were carried out. The calculations were limited to **3**X *anti* in the conformation with Me opposite Cl, for $X^- = BF_4^-$ and BPh_4^-. For the cation, the Et, the Me, and *i*-Pr on cymene were put in the low-level layer, whereas the rest was kept in the high-level layer. For the anion, BF_4^- was kept in the high-level layer, whereas the phenyl rings on BPh_4^- were put in the low-level layer. The high-level layer was treated at the B3PW91 level. To test the influence of different types of

3BF_4 *anti*_B **3**BF_4 *anti*_A **3**BPh_4 *anti*_B **3**BPh_4 *anti*_A

Figure 11. ONIOM(B3PW91/HF) geometries of the ion pair structures with BF_4^- and BPh_4^- either on top of diimine or on top of cymene. The atoms in the low-level partition (HF) are represented with a wire frame, while the atoms in the high-level layer (B3PW91) are represented with balls and sticks.

Table 4. Relative Energies (kJ mol^{-1}) of the Different Ion Pairs Calculated at the ONIOM Level with Different Methods for the Low-Level Layer (ONIOM(B3PW91/UFF) and ONIOM(B3PW91/HF)), Relative Energy (kJ mol^{-1}) at the B3PW91 Level on the ONIOM(B3PW91/HF) Geometries with Inclusion of the Solvent Effect (CH_2Cl_2) as a Continuum PCM Model, Formation Energy E_b (kJ mol^{-1}) of the Various Ion Pairs from PCM(B3PW91/CH_2Cl_2) Energy Calculations of the Ion Pair, the Cation, and the Anion in the Geometry They Have in the Ion Pair

	3BF_4 *anti*_B	**3**BF_4 *anti*_A	**3**BPh_4 *anti*_B	**3**BPh_4 *anti*_A
ONIOM(B3PW91/UFF)	0.0	35.9	0.0	−9.8
ONIOM(B3PW91/HF)	0.0	62.2	0.0	4.5
PCM(B3PW91/CH_2Cl_2)	0.0	37.2	0.0	7.1
E_b (PCM/CH_2Cl_2)	98.1	51.7	36.4	28.2

interactions on the structure and energetics of the ion pair, two different methods were used to describe the low-level layer: molecular mechanics with the UFF force field and Hartree−Fock.

Only the two relative orientations of the anion and the cation observed in the solid state were considered: anion on top of the diimine ligand (**3**BF_4 *anti*_B and **3**BPh_4 *anti*_B) and anion on top of the cymene ring (**3**BF_4 *anti*_A and **3**BPh_4 *anti*_A). The geometries obtained with ONIOM(B3PW91/HF) calculations are shown in Figure 11, and the relative energies between the ion pairs are reported in Table 4.

The ONIOM calculations clearly indicate a strongly preferred ion pair structure with BF_4^- and two ion pairs of similar energy with BPh_4^-. For BF_4^-, the ion pair structure with the anion close to the diimine ligand and to the cymene methyl group (**3**BF_4 *anti*_B) is significantly more stable than the ion pair structure with the anion sitting on top of the cymene ligand (**3**BF_4 *anti*_A). The energy difference is more pronounced at the ONIOM(B3PW91/HF) level (62.2 kJ mol^{-1}) than at the ONIOM(B3PW91/UFF) level (35.9 kJ mol^{-1}). Inclusion of the solvent effects as a continuum still preserves **3**BF_4 *anti*_B as the most stable ion pair structure. The PCM calculations allow the formation energy of the ion pair to be estimated as the difference between the ion pair energy and the energies of both the anion and cation in the ion pair geometry (Table 4). Strictly speaking, this is not a formation energy because the fragments are not in their optimized geometry, but it gives a good estimate of the energy range involved in the ion pair formation process. In the case of **3**BF_4 *anti*_B, the value of 98.1 kJ mol^{-1} is in agreement with the ion pair formation being mainly driven by H-bonding interactions. As a matter of fact several short F···H contacts are present in the ion pair. The shortest contacts are with the methyl groups on the diimine backbone (2.071 Å, H8; 2.074 Å, H8′), followed by similar contacts with H11′ (2.268 Å), H5 (2.357 Å), and H16 (2.306 Å). These values are in qualitative agreement with the relative values for the NOE intensities in the $^{19}F,^1H$-HOESY spectrum for **3**BF_4 *anti* (Table 2). In the present ONIOM(B3PW91/HF) calculations, the F···H interactions are described at the DFT level for the F···H8 and F···H8′ contacts, whereas the F···H contacts with H11′, H5, and H16 are described at HF. This might explain in part the discrepancies between the respective trends both in the NOE intensities and in the contact values. This is further confirmed by the results from the ONIOM(B3PW91/UFF) calculations on **3**BF_4 *anti*_B, where F···H8 and F···H8′ contacts are still described at the DFT level, whereas the F···H11′, F···H5, and F···H16 contacts are treated only at the UFF level and no correct description of the H-bonding interaction is expected. The F···H8 and F···H8′ are shorter than in the ONIOM(B3PW91/HF) calculations (1.973 Å, H8; 1.986 Å, H8′) and longer for the other contacts (2.462 Å, H11′; 2.710 Å, H5; 2.390 Å, H16). As a consequence, the energy difference between the two ion pair structures with BF_4^- is smaller because there is less stabilization through H-bonding interactions.

For the ion pair with BPh_4^-, the driving forces of the ion pair formation are either π-stacking interactions between the phenyl rings on BPh_4^- and cymene or C−H···π interactions between the diimine methyl groups and phenyl groups on BPh_4^-. For the ion pair **3**BPh_4 *anti*_B, the phenyl ring below the two diimine methyl groups exhibits two short H···centroid distances of 3.305 Å (H8) and 3.368 Å (H8′), whereas the one facing the diimine ligand and pointing toward the cymene exhibits a shorter H···centroid distance with H8′ (2.963 Å) than with H8 (3.553 Å) because of the asymmetry imposed by the ethyl chain. These stacking interactions are all described at the HF level due to the choice made for the partition. In the ONIOM(B3PW91/UFF) calculations some of these contacts are shorter (2.84 Å for the phenyl group below, 2.711 Å for the phenyl group facing) because these stacking interactions are described by UFF.

The other ion pair with BPh_4^- on top of the cymene (**3**BPh_4 *anti*_A) is calculated to be of similar energy (Table 4) because the ion pair stability is due to the same type of interactions. The centroid−centroid distance between the two phenyl rings that are almost parallel (cymene and BPh_4^- phenyl rings) is 4.4 Å, a value indicative of the presence of π-stacking interactions. The H···centroid contacts between H2 and H3 and the phenyl ring of the side of the cymene ring are also rather short (3.393 Å, H2; 3.422 Å, H3). The H5···centroid contact with the phenyl ring on top of the cymene is of the same order of magnitude (3.407 Å). In the case of the ONIOM(B3PW91/UFF) calculations, these contacts are shorter, with a centroid−centroid distance of 3.686 Å and H2···centroid and

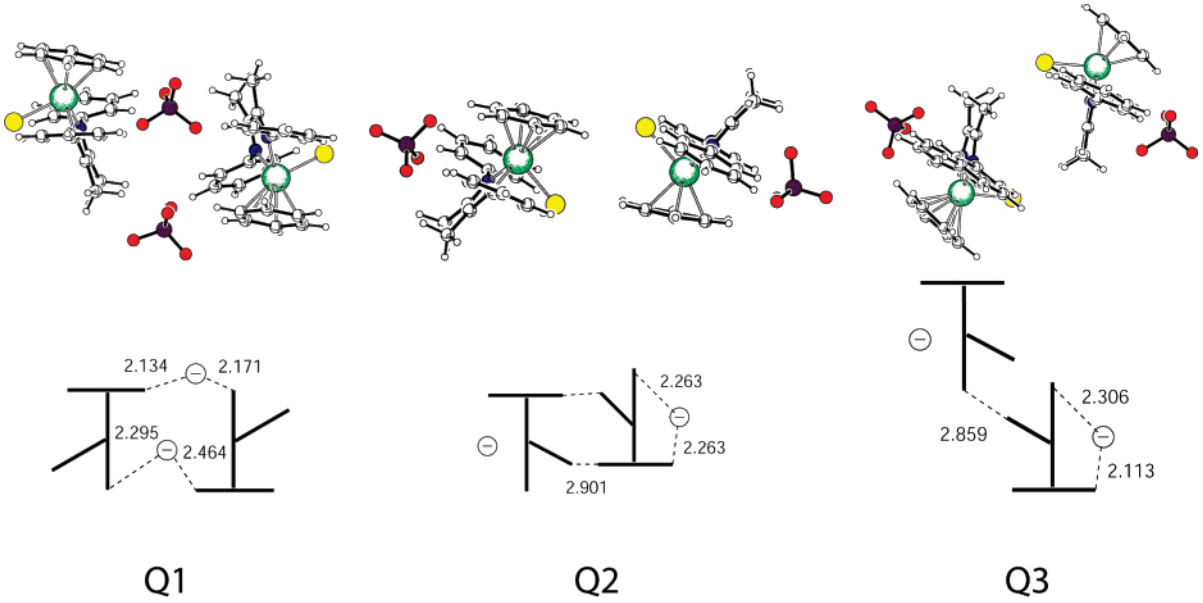

Figure 12. The three different structures of ion quadruples considered (**Q1**, **Q2**, and **Q3**) together with a schematic representation that highlights the basic interaction patterns. On each schematic representation the shortest contact with H involving either F (anion) or Cl is shown.

H3···centroid contacts of 2.912 and 3.174 Å, respectively. This overestimation of the stacking interactions is the result of **3**BPh_4 *anti*_A being more stable than **3**BPh_4 *anti*_B in the ONIOM-(B3PW91/UFF) calculations, while **3**BPh_4 *anti*_B is more stable in the ONIOM(B3PW91/HF) calculations (Table 4). Nevertheless the energy differences are small and the two ion pair structures are best considered as isoenergetic, in agreement with the ^{1}H-NOESY experiments where contacts with cymene and diimine protons were of similar intensities.

In contrast to the BF_4^- anion held in a specific position as the result of cooperative H-bonding interactions with the fluorine atoms, the BPh_4^- anion is engaged in less directional and weaker stacking interactions and thus does not form a single ion pair with a precise geometry. This is illustrated by the lower value of the formation energy of the ion pair either at the diimine (36.4 kJ mol^{-1}) or at the cymene (28.2 kJ mol^{-1}). Breaking the ion pair with BF_4^- is thus expected to be energetically demanding, and the formation of higher order aggregates may need to maintain this favorable motif.

Structure and Energetics of the Quadrupoles. The PGSE experiments indicated the presence of ion quadruples in solvent with low relative permittivity such as chloroform and benzene. To shed more light on the structure and energetics of the various quadrupoles with small and fluorinated counterions, DFT calculations were carried out. Due to the size of the system, only the simplest complex, **5**BF_4, was considered. Following the observations from X-ray solid-state investigations, three different structures of ion quadruples were considered (Figure 12): **Q1** having two bridging BF_4^- anions (observed in the solid state for **5**PF_6, Figure 9 top right), **Q2** containing Ru−Cl···H−C(cymene) intercationic interactions (observed in the solid state for **2**BF_4 *syn*, Figure 9 bottom left), and **Q3** containing Ru−Cl···H−CH_2(diimine) intercationic interactions (observed in the solid state for **5**PF_6, Figure 9 bottom right). The relative energies of the quadrupoles in the gas phase and in CH_2Cl_2 (PCM single-point calculations on gas-phase-optimized geometries) are given in Table 5.

The calculations on the ion pairs show the strong interaction of BF_4^- with both the diimine and cymene ligands. It is thus expected that the formation of quadrupoles would tend to maintain this preferred interaction, as observed in the three optimized quadrupoles. The most stable situation, **Q1**, is obtained when a unique BF_4^- is engaged in two such interactions, leading to the expected cation−anion−cation sequence. However, such a pattern develops at the expense of the second anion that finds stabilizing interactions with the η^6-C_6H_6 and diimine methyl groups slightly above the aforementioned tripole. The two other quadrupoles preserve the preferred interactions for each BF_4^-, thus leading to the anion−cation−cation−anion sequence. The main difference between **Q2** and **Q3** lies in the way the two cations interact. In **Q2**, the chlorine atom is interacting with H atoms on the η^6-C_6H_6 group in a typical inverted piano stool geometry. In **Q3**, the shortest Cl···H contacts are with the diimine methyl groups.

Table 5. B3PW91 Relative Energies (kJ mol^{-1}) in Gas Phase (E_{GP}) and in CH_2Cl_2 (E_{PCM}) for the Three Quadrupoles, and Formation Energy in Gas Phase ($\Delta_f E_{GP}$) and in CH_2Cl_2 ($\Delta_f E_{PCM}$)

	Q1	Q2	Q3
E_{GP}	0.0	21.2	23.0
E_{PCM}	0.0	9.7	3.8
$\Delta_f E_{GP}$	−47.2	−26.0	−24.2
$\Delta_f E_{PCM}$	−20.6	−10.9	−16.8

In the gas phase, **Q1** is significantly more stable than the other two quadrupoles, the latter two being of similar energy (Table 5). Inclusion of solvent effects as a continuum reduces the energy differences between the various quadrupoles, with **Q1** still the most stable structure. The energy differences are small enough that the actual geometry in solution or in the solid state may depend critically on the steric bulk of both the anion (BF_4^- versus PF_6^-) and the cation (cymene versus benzene and alkyl chain on phenyl diimine groups).

To evaluate the formation energy of the quadrupole, the ion pair structure, **IP**, with the present simplified model was optimized. The latter presents the basic interaction features obtained for **3**BF_4 *anti*_B. The formation energy of the ion pair was calculated to be 105.2 kJ mol^{-1}, a value similar to that obtained for **3**BF_4 *anti*_B (98.1 kJ mol^{-1}). For the quadrupoles, the formation energy from the neutral ion pair can be evaluated in the gas phase and in CH_2Cl_2 (Table 5). Interestingly, the

quadrupole formation process is exothermic for all the isomers, in the gas phase and in solvent. Thus there is an energetic driving force toward higher order aggregation. The formation energy of **Q1** is significantly lowered in CH_2Cl_2 compared to the gas-phase values because both BF_4^-'s are interacting with both cations and are partially shielded from the solvent in the quadrupole. The solvent−anion interaction (even described as a continuum) in **IP** is lost in **Q1**, thus leading to a lower formation energy. The situation is slightly different for **Q2** and **Q3** because the anion occupies a position that is similar in the ion pair and in the quadrupole. The lowering of the formation energy is thus less important. The inverted piano stool geometry corresponds to a chlorine atom that is more buried inside the quadrupole, and thus the formation energy is more strongly influenced by the shift from the gas phase to CH_2Cl_2. Nevertheless, the formation energy values of the three quadrupoles are sufficiently similar so as to exclude the preference for anyone particular geometry. Depending on the actual nature of the system, the three situations may occur; however a shift toward **Q2** and **Q3** is anticipated when the steric bulk of the anion and/or the cation is increased.

Discussion

An integrated approach for investigating the aggregation of transition-metal salts in solution appears to be particularly promising due to the complementary information obtainable from the various techniques. PGSE NMR measurements are crucial for estimating the average size of the ionic adducts in solution, thus identifying their nature, while NOE NMR experiments allow the relative orientation(s) of the ionic moieties within the adducts to be determined. From interionic X-ray studies, the metric parameters of the interionic adduct can be evaluated. Several anion cation orientations are present in the solid state, and even though they may be absent in solution, they surely provide a good starting point for comparative considerations. The crucial link between the solid-state structure of interionic adducts and that observed solution is given by calculations (ONIOM or DFT).

The PGSE NMR experiments indicate the ionic form in which complexes **1**−**3**X are present in solution, thus affording the initial information that is necessary to determine their interionic structure. The aggregation tendency of complexes **1**−**3**X depends on the solvent, concentration, and counterion as described in earlier. Not surprisingly, *ion pairing* is *the main aggregation process in CD_2Cl_2 or in solvents with a ϵ_r higher than that of CD_2Cl_2*. However, in addition to the polarity, the nature of the solvent is also important in determining the aggregation process. This is clearly demonstrated by comparing the PGSE results in isodielectric solvents acetone-d_6 and 2-propanol-d_8 for complex **3**BF_4 *anti*: the aggregation tendency is higher in the latter. Although a little counterintuitive, this behavior has been observed for NBu_4X salts through conductivity measurements.[19,20] Both concentration and counterion effect on ion pairing of complexes **1**−**3**X are standard in that ion pairing is favored by "more coordinating" conterions and an increase of the concentration. In reality, it would be more correct to speak about "ion-pairing tendency" than "coordinating tendency", since in the ion pairs of complexes **1**−**3**X the counterion stays on the second coordination sphere of the saturated cations and, consequently, they are OSIPs. This distinction is critical, especially for the position in the scale of BPh_4^- that, when paired with an unsaturated cation, may afford ISIPs more easily than BF_4^- and PF_6^- through η^2- or η^6-coordination and the possible subsequent transfer of an aryl ring.[25] Recently, Weller and co-workers showed that η^6-coordination can also occur for $BARF^-$.[26]

***1*-*3*X OSIPs aggregate, in benzene-d_6 and chloroform-*d*, to form ion quadruples**. Although a complete study could not be done due to the insolubility of some salts, an interesting result was obtained. *The counterion effect on the formation of ion quadruples from ion pairs is the opposite of what occurs on the formation of ion pairs from free ions*. In fact, the tendency to form ion quadruples in chloroform-*d* and benzene-d_6 is $BPh_4^- > CF_3SO_3^- \approx BF_4^-$ and $BARF^- > PF_6^-$, respectively. Large counterions probably do not have the possibility to suitably dock with the cation, and the resulting OSIPs have a higher dipolar moment than those with small counterions. This high dipolar moment may facilitate their aggregation to ion quadruples. In agreement, the dipole moment of **3**BF_4 *anti* with the anion close to the diimine ligand and **3**BPh_4 *anti* (in both A and B orientations) was estimated to be 15 and 30 D, respectively, from the PCM calculations on the ONIOM(B3PW91/HF) geometries.

Anion−Cation Orientations in Ion Pairs. The benefit of using an integrated approach to determine the anion−cation orientation in **1**−**3**X ion pairs is evident. As stated before, the PGSE results allow the right combination of solvent and concentration for having the predominance of ion pairs to be determined. For example, this occurs for all complexes (except **1**BARF) in CD_2Cl_2 at ca. 10 mM. For complexes with small and fluorinated counterions, the quantification of the NOEs clearly indicated that the anion specifically "sits" over the N═C−C═N moiety of the diimine ligand (orientation B). X-ray studies on **2**BF_4 *syn* and **5**PF_6 showed that this relative anion−cation orientation is actually present in the solid state with Ru···B and Ru···P distances equal to 6.06 and 5.23 Å, respectively. But another orientation, that for **2**BF_4 *syn* has an even shorter Ru···B distance (5.81 Å), is also present with the anion staying close to cymene (orientation A). Nevertheless, ONIOM calculations indicated that the energy of orientation B for **3**BF_4 *anti* (**3**BF_4 *anti*_B in Table 4) is at least 30.0 kJ/mol less than that of A, which validates the NMR findings.

A completely different situation was observed for **3**BPh_4 *anti*. NOE quantitative analysis of a solution for which the PGSE measurements indicated the predominance of ion pairs (Table 2, entry 47) did not allow finding a single anion−cation orientation that explained all data. In the solid state two anion−cation orientations were observed, one with the anion that exhibits $\pi-\pi$ stacking and CH−π interactions with cymene (B) and the other with the anion close to the N,N ligand (A). ONIOM calculations indicated that the two ion pairs having the anion in orientations A and B had comparable energies, supporting the idea that both of them are present in solution in similar abundance.

Structures of Ion Quadruples. As mentioned before, PGSE NMR experiments indicate that OSIPs of **1**−**3**X complexes aggregate in low-polarity solvents such as chloroform-*d* and benzene-d_6, affording ion quadruples. While all the experimental data (X-ray and NOE NMR) strongly suggest that ion quadruples with BPh_4^- anions are constituted by an alternation of cations and anions, they do not provide an explanation for the structure of ion quadruples with small and fluorinated counterions. Interionic NOE intensities are almost invariant on passing from ion pairs to ion quadruples, even if a small increase of interionic NOEs with arene protons suggests an average shift

(25) Strauss, S. H. *Chem. Rev.* **1993**, *93*, 927.
(26) Douglas, T. M.; Molinos, E.; Brayshaw, S. K.; Weller, A. S. *Organometallics* **2007**, *26*, 463−465.

of the counterions toward cymene. X-ray studies suggest at least four possible structures of ion quadruples (Figure 9) differing in both disposition and orientation of the ionic moieties. Leaving the counterion in the favorable B orientation, two ion pairs can aggregate using the counterions as bridges ($Ru^+X^-X^-Ru^+$, Figure 9 top) or through intercationic interactions ($X^-Ru^+Ru^+X^-$, Figure 9 bottom). DFT calculations carried out on the simplest complex (arene = benzene, R = H, and $X^- = BF_4^-$) show that the aggregation of two ion pairs forming any type of the considered ion quadruples is an exothermic process. **Q1** ($Ru^+X^-X^-Ru^+$) ion quadruple is slightly favored in energy (Table 5), but the energy differences are so small that they can be overcome by introducing different arene or R substituents or counterions. Moreover, the small increase of NOE intensities of the BF_4^-/cymene protons on passing from ion pairs to ion quadruples for **3**BF_4 *anti* suggests that **Q1** is the most probable structure for ion quadruples, at least in this complex. In fact, due to the steric hindrance of *ortho*-Et substituents and cymene, the association of two ion pairs on the side of the diimine ligand bearing BF_4^- could cause a slight shift of the counterion toward cymene.

Conclusions

Herein we have shown how an integrated experimental and theoretical approach has allowed an in-depth description of the interionic structure of [Ru(η^6-Arene){(2-R-C_6H_4)N=C(Me)−C(Me)=N(2-R-C_6H_4)}Cl]X (**1**−**5**X) complexes to be obtained.

PGSE NMR experiments were of crucial importance for understanding the ionic forms that were mainly present in solution. Having found the correct conditions (solvent, counterion, and concentration) needed to obtain the predominance of ion pairs and ion quadruples, their structure was investigated by combining NOE NMR experiments, X-ray studies, and calculations (DFT and ONIOM).

In **1**−**5**X ion pairs with small, fluorinated counterions, there is a strong preference for the anion to locate above the plane containing the C=N imine moieties. When ion pairs aggregate forming ion quadruples (in chloroform-*d* and benzene-d_6), they try to maintain such an anion−cation orientation. In cases of small counterions and substituents, "$Ru^+X^-X^-Ru^+$" ion quadruples may form. Otherwise, "$X^-Ru^+Ru^+X^-$" ion quadruples, stabilized by Ru−Cl···H−C intercationic interactions, are probably favored. In both cases, calculations indicated that the formation of an ion quadruple from two ion pairs is an exothermic process.

When BPh_4^- counterion is used, two anion−cation orientations are almost isoenergetic in ion pairs. The anion is positioned (a) on the side of the cymene ligand and orients a phenyl ring almost coplanarly with the cymene ring to give $\pi-\pi$ stacking interactions or (b) on the side of the N,N ligand and shows contacts between the three hydrogen atoms of the imine methyls and the phenyl group. An alternation of anion and cation occurs in ion quadruples.

It should be noted that the tendency to form ion quadruples from ion pairs increases when "least" coordinating counterions are used. This leads to a higher charge separation in ion pairs with a consequent enhanced molecular dipole moment and aggregation tendency.

Experimental Section

General Procedures. The synthesis of 1,4-diazabutadiene ligands (2-R-C_6H_4)N=C(Me)−C(Me)=N(2-R-C_6H_4) was performed according to the literature procedures.[15,27] $RuCl_3 \cdot 3H_2O$ was purchased from Sigma, and the ruthenium chlorine dimers were prepared according to Benneth et al.[28]

The preparation of compounds was carried out under nitrogen using standard Schlenk techniques. The compounds were prepared using freshly distilled solvents (hexane with Na, Et_2O with Na/benzophenone, MeOH with CaH_2, CH_2Cl_2 and CH_3CN with P_2O_5). The solvents were also degassed by many gas−pump−nitrogen cycles before use.

One- and two-dimensional ^1H, ^{13}C, ^{19}F, and ^{31}P NMR spectra were measured on Bruker DPX 200 and DRX 400 spectrometers. Referencing is relative to TMS (^1H and ^{13}C), CCl_3F (^{19}F), and 85% H_3PO_4 (^{31}P). NMR samples were prepared by dissolving the suitable amount of compound in 0.5 mL of deuterated solvent.

Synthesis of Complex 1BPh$_4$. Method a. A 0.537 g (0.877 mmol) sample of the dimer [Ru(η^6-arene)Cl_2]$_2$ and 0.404 g (1.754 mmol) of the ligand PhN=C(Me)-C(Me)=NPh were suspended in 5 mL of MeOH. The suspension was stirred for many hours (3−6) at rt until the color of the solution changed from red-orange to brown; a large excess of $NaBPh_4$ (10 equiv) in 0.5 mL of MeOH was added and a precipitate formed. The solution was filtered, and the solid was washed with cold MeOH and *n*-hexane. Yield = 96%. Slow diffusion of ether into a CH_2Cl_2 solution of the complexes produced red crystals.

Method b. A 0.071 g (0.119 mmol) portion of **1**BF_4 was dissolved in 5 mL of MeOH. A large excess of $NaBPh_4$ (10 equiv) in 0.5 mL of MeOH was added, and a precipitate formed. The solution was filtered, and the solid was washed with cold MeOH and *n*-hexane. Yield = 96%. Slow diffusion of ether into a CH_2Cl_2 solution of the complexes produced red crystals. The complex was obtained with the same procedure but with the use of **1**PF_6 instead of **1**BF_4.

^1H NMR (CD_2Cl_2, 298 K, 400.13 MHz, *J* in Hz): δ 1.10 (d, $^3J_{H7-H6}$ = 6.9, H7), 2.05 (s, H5), 2.20 (s, H8), 2.55 (sept., H6), 4.80 (d, $^3J_{H3-H2}$ = 6.4, H3), 4.93 (d, $^3J_{H2-H3}$ = 6.4, H2), 6.90 (t, $^3J_{p-m}$ = 7.1, *p*), 7.04 (t, $^3J_{m-o} = {}^3J_{m-p}$ =7.4, *m* and H11or H15), 7.34 (br, *o*), 7.56 (dd, $^3J_{H13-H14}$ = 8.5, $^4J_{H13-H11}$ = 2.0, H13), 7.65 (t, $^3J_{H12-H13,H11} = {}^3J_{H12-H11}$ = 8.0, H12), 7.71 (br, H11 or H15). $^{13}C\{^1H\}$ NMR (CD_2Cl_2, 298 K): δ 20.7 (s, C8), 22.3 (s, C7), 31.4 (s, C6), 88.3 (s, C2), 88.5 (br, C3), 105.5 (s, C1), 110.8 (s, C4), 119.6 (s, C11 or C15), 122.1 (s, *p*), 122.4 (s, C11 or C15), 125.0 (q, $^3J_{m-B}$ = 5.23, *m*), 129.8 8 (s, C12 or C14), 130.0 (s, C13), 130.9 (s, C12 or C14), 136.3 (s, *o*), 151.3 (s, C10), 164.4 (q, $^1J_{C-B}$ = 49.2, C-*ipso*), 176.7 (s, C9). Anal. Calcd (%) for $C_{50}H_{50}BClN_2Ru$ (826.3): C 72.68, H 6.10, N 3.39. Found: C 72.54, H 6.04, N 3.32.

Synthesis of Complex 1BF$_4$. Method c. A 0.537 g (0.877 mmol) sample of the dimer [Ru(η^6-arene)Cl_2]$_2$ and 0.404 g (1.754 mmol) of the ligand PhN=C(Me)−C(Me)=NPh were dissolved in 10 mL of CH_2Cl_2, and 0.345 g of $AgBF_4$ (1.754 mmol) was added under a nitrogen atmosphere. The solution immediately changed from red to brown, and a AgCl precipitate formed. The solution was filtered and dried under vacuum, and a red solid was obtained. Yield = 90%. Slow diffusion of ether into a CH_2Cl_2 solution of the complexes produced red crystals.

Method d. A 0.100 g (0.877 mmol) amount of **1**BPh_4 was dissolved in 5 mL of CH_2Cl_2. Then 0.345 g of $AgBF_4$ (1.754 mmol) was added under a nitrogen atmosphere, and a $AgBPh_4$ precipitate

(27) (a) tom Dieck, H.; Kinzel, A. *Angew. Chem.* **1979**, *91*, 344. (b) Diercks, R.; Stamp, L.; Kopf, J.; tom Dieck, H. *Angew. Chem.* **1984**, *961*, 891. (c) Wu, C.; Swift, H. *J. Catal.* **1972**, *24*, 510. (d) Naly, N. A. U.S. Patent 3446862; *Prepr. Am. Chem. Soc., Div. Pet. Chem.* **1972**, *17*, B95. (e) tom Dieck, H.; Bruder, H. *J. Chem. Soc., Chem. Commun.* **1977**, 24. (f) Cotton F. A.; Wilkinson, G. *Advanced Inorganic Chemistry*, 5th ed.; Wiley-Interscience: New York, 1988; p 40.

(28) Benneth, M. A.; Smith, A. K. *J. Chem. Soc., Dalton Trans.* **1974**, 233.

formed. The solution was filtered and dried under vacuum, obtaining a red solid. Yield = 98%. Slow diffusion of ether into a CH_2Cl_2 solution of the complexes produced red crystals. ^{1}H NMR (CD_2Cl_2, 298 K, 400.13 MHz, *J* in Hz): δ 1.10 (d, $^3J_{H7-H6}$ = 6.9, H7), 2.06 (s, H5), 2.37 (s, H8), 2.66 (sept., J_{H6-H7} = 6.9, H6), 4.94 (d, $^3J_{H3-H2}$ = 6.4, H3), 4.97 (d, $^3J_{H2-H3}$ = 6.4, H2), 7.43 (br, H11 or H15), 7.52 (dd, $^3J_{H13-H12}$ = 8.0, $^4J_{H13-H11}$ = 1.2, H13), 7.65 (br, H12 and H11 or H15). ^{19}F NMR (CD_2Cl_2, 298 K): δ −151.8 (br,$^{10}BF_4$), −151.9(br, $^{11}BF_4$). Anal. Calcd (%) for $C_{26}H_{30}BClF_4N_2Ru$ (593.9): C 52.58, H 5.09, N 4.72. Found: C 52.50, H 5.03, N 4.78.

Synthesis of Complex 1PF$_6$. The **1**PF_6 complex was obtained with the same procedures (c and d) as **1**BF_4, but $TlPF_6$ was used instead of $AgBF_4$. ^{1}H NMR (CD_2Cl_2, 298 K, 400.13 MHz, *J* in Hz): δ 1.10 (d, $^3J_{H7-H6}$ = 6.9, H7), 2.06 (s, H5), 2.37 (s, H8), 2.66 (sept., J_{H6-H7} = 6.9, H6), 4.94 (d, $^3J_{H3-H2}$ = 6.4, H3), 4.97 (d, $^3J_{H2-H3}$ = 6.4, H2), 7.43 (br, H11 or H15), 7.52 (dd, $^3J_{H13-H12}$ = 8.0, $^4J_{H13-H11}$ = 1.2, H13), 7.65 (br, H12 and H11 or H15). ^{13}C-{^{1}H} NMR (CD_2Cl_2, 298 K): δ 20.7 (s, C8), 22.3 (s, C7), 31.4 (s, C6), 88.3 (s, *C*2), 88.5 (br, C3), 105.5 (s, C1), 110.8 (s, C4), 119.6 (s, C11 or C15), 122.1 (s, *p*), 122.4 (s, C15 or C11), 125.0 (br, *m*), 129.8 (s, C12 or C14), 130.0 (s, C13), 130.9 (s, C14 or C12), 136.3 (s, *o*), 151.3 (s, C10), 164.4 (q, $^1J_{C-B}$ = 49.2, C-*ipso*), 176.7 (s, C9). ^{19}F NMR (CD_2Cl_2, 298 K): δ −72.1 (d, $^1J_{FP}$ = 711). ^{31}P NMR (CD_2Cl_2, 298 K): δ −143.2 (sept, $^1J_{PF}$ = 711). Anal. Calcd (%) for $C_{26}H_{30}ClF_6N_2PRu$ (652.0): C 47.89, H 4.64, N 4.30. Found: C 47.81, H 4.68, N 4.25.

Synthesis of Complex 1BARF. Method c. A 0.075 g (0.123 mmol) sample of the dimer $[Ru(\eta^6\text{-arene})Cl_2]_2$ and 0.116 g (0.492 mmol) of the ligand PhN═C(Me)−C(Me)═NPh were dissolved in 5 mL of CH_2Cl_2. Then 0.229 g of NaBARF (0.258 mmol) was added under a nitrogen atmosphere, and a NaCl precipitate formed. The solution was filtered and then *n*-hexane was added and a brown solid formed. The solution was filtered again, and the solid was washed with *n*-hexane. Yield = 85%. Slow diffusion of *n*-hexane into a CH_2Cl_2 solution of the complexes produced brown crystals. ^{1}H NMR (CD_2Cl_2, 298 K, 400.13 MHz, *J* in Hz): δ 1.10 (d, $^3J_{H7-H6}$ = 7.2, H7), 2.14 (s, H5), 2.35 (s, H8), 2.57 (sept, $^3J_{H6-H7}$ = 7.2, H6), 4.86 (d, $^3J_{H3-H2}$ = 6.3, H3), 4.98 (d, $^3J_{H2-H3}$ = 6.2, H2), 7.09 (m, H11), 7.53 (t, $^3J_{H13-H14,H12}$ = 7.3, H13), 7.60 (s, *p*), 7.65 (m, H12, H14, H15), 7.76 (s, *o*). ^{19}F NMR (CD_2Cl_2, 298 K): δ −62.71 (s, CF_3). Anal. Calcd (%) for $C_{58}H_{42}BClF_{24}N_2Ru$ (1370.26): C 50.84, H 3.09, N 2.04. Found: C 50.88, H 3.01, N 2.09.

Synthesis of Complex 2-5X (X = BPh$_4$, BF$_4$, PF$_6$, CF$_3$SO$_3$, BARF). Complexes **2**−**5**X (X = BPh_4, BF_4, PF_6, CF_3SO_3, BARF) were obtained with the same procedures (a−d) for **1**X by using the appropriate ligand (2-R-C_6H_4)N═C(Me)−C(Me)═N(2-R-C_6H_4). In those cases two isomers, *anti* and *syn*, were formed in a 2:1 ratio, and the yields ranged from 85% to 95%. Slow diffusion of *n*-hexane or ether into a CH_2Cl_2 solution of mixtures of the two isomers allowed the *anti* or *syn* isomers to be isolated when X^- = BPh_4^- or X^- = BF_4^-, PF_6^-, and $CF_3^-SO_3^-$, respectively. In the selected NMR data, when present, **a** indicates the *anti* isomer and **s** indicates the *syn* isomer.

2BPh$_4$. ^{1}H NMR (CD_2Cl_2, 298 K, 400.13 MHz, *J* in Hz): δ 1.07 (d, $^3J_{H7'-H6}$ = 6.9, H7′(**a**)), 1.14 (d, $^3J_{H7-H6}$ = 6.9, H7(**s**)), 1.16 (d, $^3J_{H7-H6}$ = 6.9, H7(**a**)), 1.82 (s, H5(**s**)), 1.88 (s, H5(**a**)), 2.13 (s, H8′(**a**)), 2.16 (s, H8(**s**) and H8(**a**)), 2.22 (s, 16(**s**) and 16-(**a**)), 2.40 (s, 16′(**a**)), 2.43 (m, H6(**s**) and H6(**a**)), 4.82 (dd, $^3J_{H3-H2}$ = 6.1, H3(**a**)), 4.89, (dd, $^4J_{H2'-H6}$ = 1.1, H2′(**a**)), 4.90 (d, $^3J_{H3-H2}$ = 6.4, H3(**s**)), 4.975 (dd, $^3J_{H3'-H2'}$ = 6.1, $^4J_{H3'-H5}$ = 1.4, H3′(**a**)), 4.98 (d, $^3J_{H2-H3}$ = 6.3, H2(**s**)), 5.09 (dd, $^3J_{H2-H3}$ = 6.2, $^4J_{H2-H6}$ = 1.0, H2(**a**)), 6.89 (t, $^3J_{m-p}$ = 7.1, *p* and H11′(**a**)), 7.03 (t, $^3J_{m-o,p}$ = 7.4, *m*), 7.52 (br, *o*), 7.49 (m, H14 and H12 and H11(**s**) and H14 and H14′(**a**) and H13 and H13′(**a**) and H12 and H12′(**a**)), 7.73 (m, H11(**s**)), 7.92 (m, H11(**a**)). Anal. Calcd (%) for $C_{52}H_{54}BClN_2Ru$ (854.3): C 73.10, H 6.37, N 3.28. Found: C 73.18, H 6.31, N 3.23.

3BPh$_4$ *anti*. ^{1}H NMR (CD_2Cl_2, 298 K, 400.13 MHz, *J* values in Hz): δ 1.11 (d, $^3J_{H7'-H6}$ = 6.96, H7′), 1.13 (d, $^3J_{H7-H6}$ = 6.89, H7), 1.21 (t, $^3J_{H17'-H16'}$ = 7.51, H17′), 1.46 (t, $^3J_{17-16}$ = 7.53, H17), 1.90 (s, H5), 2.13 (s, H8′), 2.16 (s, H8), 2.40 (m, H16 and H6), 2.50 (m, $^2J_{H16-H16}$ = 14.8, $^3J_{H16-H17}$ = 7.47, H16), 2.78 (m, $^2J_{H16'-H16'}$ = 14.8, $^3J_{H16'-H17'}$ = 7.4, H16′), 3.00 (m, $^2J_{H16'-H16'}$ = 14.8, $^3J_{H16'-H17'}$ = 7.4, 16′), 4.81 (dd, $^3J_{H3'-H2'}$ = 6.27, $^4J_{H3'-H5}$ = 1.10, H3′), 4.88 (dd, $^3J_{H2-H3}$ = 6.21, $^4J_{H2-H6}$ = 1.25, H2), 4.91 (dd, $^3J_{H3-H2}$ = 6.19, $^4J_{H3-H5}$ = 1.04, H3), 4.96 (dd, $^3J_{H2'-H3'}$ = 6.28, $^4J_{H2'-H6}$ = 1.26, H2′), 6.84 (dd, $^3J_{H11'-H12'}$ = 7.71, $^4J_{H11'-H13'}$ = 1.36, H11′), 6.90 (t, $^3J_{p-m}$ = 7.32, *p*), 7.03, (t, $^3J_{m-o,p}$ = 7.41, *m*), 7.31 (br, *o*), 7.49 (m, H12 and H12′), 7.54 (m, H13 and H13′), 7.59 (m, H14′), 7.61 (m, H14), 7.88 (dd, $^3J_{H11-H12}$ = 7.90, $^4J_{H11-H13}$ = 1.32, H11). ^{13}C{^{1}H} NMR (CD_2Cl_2, 298 K, 100.55 MHz): δ 13.7 (s, 17), 15.1 (s, 17′), 18.7 (s, C5), 21.1 (s, C8), 21.6 (s, C8′), 21.8 (s, C7′), 21.5 (s, C7), 23.2 (s, 16), 25.2 (s, 16′), 31.1 (s, C6), 85.2 (s, C2), 85.9 (s, C2′), 88.9 (s, C3′), 91.1 (s, C3), 103.8 (s, C1), 114.8 (s, C4), 121.5 (s, C11), 122.1 (s, *p*), 122.2 (s, C11′), 126.0 (q, *m*), 127.6 (C12 or C12′), 128.0 (s, C12′ or C12), 129.0 (s, C14′), 129.8 (s, C13 or C13′), 130.1 (s, C13′ or C13), 131.6 (s, C14), 132.4 (s, C15′), 136.3 (q, $^2J_{o-B}$ = 2.8, *o*), 137.2 (s, C15), 149.2 (s, C10), 149.9 (s, C10′), 164.4 (q, $^1J_{C-B}$ = 49.2, C-*ipso*), 177.8 (s, C9), 178.7 (s, C9′).

3BPh$_4$ *syn*. ^{1}H NMR (CD_2Cl_2, 298 K, 400.13 MHz, *J* values in Hz): δ 1.12 (d, $^3J_{H7-H6}$ = 6.96, H7), 1.45 (t, $^3J_{17-16}$ = 7.53, 17), 1.80 (s, H5), 2.18 (s, H8), 2.43 (m, 16 and H6), 4.91 (d, $^3J_{H3-H2}$ = 6.27, H3), 4.97 (d, $^3J_{H2-H3}$ = 6.21, H2), 6.90 (t, $^3J_{p-m}$ = 7.32, *p*), 7.03, (t, $^3J_{m-o,p}$ = 7.41, *m*), 7.31 (br, *o*), 7.48 (ddd, $^3J_{H12-H13}$ = 7.9, $^3J_{H12-H11}$ = 7.8, $^4J_{H12-H14}$ = 1.5, H12), 7.53 (ddd, $^3J_{H13-H12}$ = 7.9, $^3J_{H13-H14}$ = 7.2, $^4J_{H13-H11}$ = 1.2, H13), 7.61 (dd, $^3J_{H14-H13}$ = 7.2, $^4J_{H14-H12}$ = 1.5, H14), 7.71 (dd, $^3J_{H11-H12}$ = 7.8, $^4J_{H11-H13}$ = 1.2, H11). ^{13}C{^{1}H} NMR (CD_2Cl_2, 298 K, 100.55 MHz): δ 13.6 (s, 17), 18.6 (s, C5), 20.9 (s, C8), 22.1 (s, C7), 23.2 (s, 16), 31.1 (s, C6), 85.9 (s, C2), 89.9 (s, C3), 103.6 (s, C1), 115.0 (s, C4), 122.1 (s, C11 and *p*), 126.0 (q, *m*), 128.1 (s, C12), 129.0 (s, C14), 129.8 (s, C13), 132.1 (s, C15), 136.2 (q, $^2J_{o-B}$ = 2.8, *o*), 149.3 (s, C10), 164.6 (q, $^1J_{C-B}$ = 49.2, C-*ipso*), 177.7 (s, C9). Anal. Calcd (%) for $C_{54}H_{58}BClN_2Ru$ (854.3): C 73.50, H 6.63, N 3.17. Found: C 73.58, H 6.69, N 3.12.

3BF$_4$ *anti*. ^{1}H NMR (CD_2Cl_2, 298 K, 400.13 MHz, *J* values in Hz): δ 1.03 (d, $^3J_{H7-H6}$ = 6.96, H7), 1.13 (d, $^3J_{H7'-H6}$ = 6.89, H7′), 1.19 (t, $^3J_{H17'-H16'}$ = 7.51, H17′), 1.46 (t, $^3J_{H17-H16}$ = 7.53, H17), 1.95 (s, H5), 2.27 (s, H8), 2.31 (s, H8′), 2.44 (sept, $^3J_{H6-H7(H7')}$ = 6.96, H6), 2.65 (m, H16), 2.77 (m, $^2J_{H16'-H16'}$ = 14.8, $^3J_{H16'-H17'}$ = 7.47, H16′), 3.03 (m, $^2J_{H16'-H16'}$ = 14.8, $^3J_{H16'-H17'}$ = 7.47, H16′), 4.92 (d, $^3J_{H2-H3}$ = 6.27, H2), 4.98 (d, $^3J_{H3'-H2'}$ = 6.21, H3), 5.03 (m, H3 and H2′), 7.36 (dd, $^3J_{H11'-H12'}$ = 7.7, $^4J_{H11'-H13'}$ = 1.4, H11′), 7.41 (ddd, $^3J_{H12-H11}$ = $^3J_{H12-H13}$ =7.8, $^4J_{H12-H14}$ = 1.2, H12), 7.50 (m, H14′, H13, H13′, and H12′),7.60 (d, $^3J_{H14-H13}$ = 7.5, H14), 7.91 (dd, $^3J_{H11-H12}$ = 7.8, $^4J_{H11-H13}$ = 1.4, H11). ^{13}C{^{1}H} NMR (CD_2Cl_2, 298 K): δ 13.6 (s, 17), 15.1 (s, 17′), 18.2 (s, C5), 20.9 (s, C7), 21.5 (s, C7′), 21.6 (s, C8), 22.3 (s, C8′), 22.9 (s, 16), 25.2 (s, 16′), 30.8 (s, C6), 84.3 (s, C2), 85.2 (s, C2′), 88.8 (s, C3), 90.9 (s, C3′), 101.6 (s, C1), 114.6 (s, C4), 122.3 (s, C11′), 122.7 (s, C11), 127.4 (C12), 127.6 (s, C12′), 128.9, 129.6, 129.3 (s,C14, C13 and C13′), 130.9 (s, C14), 134.0 (s, C15), 136.9 (s, C15′), 149.4 (s, C10), 150.3 (s, C10′), 178.4 (s, C9), 179.7 (s, C9′). ^{19}F NMR (CD_2Cl_2, 298 K): δ −151.8 (br, $^{10}BF_4$), −151.9(br, $^{11}BF_4$).

3BF$_4$ *syn*. ^{1}H NMR (CD_2Cl_2, 298 K, 400.13 MHz, *J* values in Hz): δ 1.12 (d, $^3J_{H7-H6}$ = 6.96, H7), 1.47 (t, $^3J_{17-16}$ = 7.53, 17), 1.88 (s, H5), 2.29 (s, H8), 2.33 (sept, $^3J_{H6-H7}$ = 6.96, H6), 2.60 (m, 16), 5.02 (s,H2 and H3), 7.44 (ddd, $^3J_{H12-H13}$ = 7.9, $^3J_{H12-H11}$ = 7.8, $^4J_{H12-H14}$ = 1.5, H12), 7.51 (ddd, $^3J_{H13-H12}$ = 7.9, $^3J_{H13-H14}$ = 7.2, $^4J_{H13-H11}$ = 1.2, H13), 7.61 (dd, $^3J_{H14-H13}$ = 7.2, $^4J_{H14-H12}$

= 1.5, H14), 7.76 (dd, $^3J_{H11-H12}$ = 7.8, $^4J_{H11-H13}$ = 1.2, H11). $^{13}C\{^1H\}$ NMR (CD_2Cl_2, 298 K, 100.55 MHz): δ 13.6 (s, 17), 18.5 (s, C5), 20.9 (s, C8), 22.1 (s, C7), 23.1 (s, 16), 31.1 (s, C6), 85.7 (s, C2), 89.6 (s, C3), 103.4 (s, C1), 114.5 (s, C4), 122.1 (s, C11), 127.7 (s, C12), 129.0 (s, C14), 129.5 (s, C13), 133.2 (s, C15), 149.5 (s, C10), 178.5 (s, C9). ^{19}F NMR (CD_2Cl_2, 298 K): δ −151.8 (br, $^{10}BF_4$), −151.9(br, $^{11}BF_4$). Anal. Calcd (%) for $C_{30}H_{38}BClF_4N_2Ru$ (649.9): C 55.44, H 5.89, N 4.31. Found: C 55.51, H 5.81, N 4.37.

3CF$_3$SO$_3$ *anti*. ^1H NMR ($CDCl_3$, 298 K, 400.13 MHz, *J* in Hz): δ 1.05 (d, $^3J_{H7-H6}$ = 6.8, H7), 1.10 (d, $^3J_{H7'-H6}$ = 6.6, H7′), 1.17 (t, $^3J_{H17'-H16'}$ = 7.5, 17′), 1.49 (t, $^3J_{H17-H16}$ = 7.0, 17), 1.93 (s, H5), 2.29 (s, H8), 2.35 (s, H8′), 2.44 (sept, $^3J_{H6-H7(H7')}$ = 7.0, H6), 2.80 (m, 16′ and 16), 3.03 (m, $^2J_{H16'-H16'}$ = 14.8, $^3J_{H16'-H17'}$ = 7.5, H16′), 4.90 (d, $^3J_{H2-H3}$ = 6.3, H2), 4.98 (m, H3, H3′ and H2′), 7.34 (t, $^3J_{H12-H11,H13}$ =7.4, H12), 7.43 (m, H14′, H13, and H13′), 7.51 (t, $^3J_{H12'-H11,H13}$ = 7.6 H12′), 7.55 (d, $^3J_{H11'-H12'}$ = 4.6, H11′), 7.72 (d, $^3J_{H14-H13}$ = 6.9, H14), 7.92 (d, $^3J_{H11-H12}$ = 7.8, H11). ^{19}F NMR ($CDCl_3$, 298 K): δ −78.7 (br, CF_3). Anal. Calcd (%) for $C_{31}H_{38}ClF_3N_2O_3RuS$ (712.2): C 55.44, H 5.89, N 4.31. Found: C 55.51, H 5.81, N 4.37.

4BPh$_4$ *anti*. ^1H NMR (CD_2Cl_2, 298 K, 400.13 MHz, *J* in Hz): δ 1.10 (d, $^3J_{H18'-H16'}$ = 6.7, H18′), 1.11 (d, $^3J_{H7'-H6}$ = 6.8, H7′), 1.18 (d, $^3J_{H7-H6}$ = 7.0, H7), 1.30 (d, $^3J_{H18-H16}$ = 3.5, H18), 1.42 (d, $^3J_{H17'-H16'}$ = 6.9, H17′), 1.57 (d, $^3J_{H17-H16}$ = 6.7, 17), 1.94 (s, H5), 2.14 (s, H8′), 2.16 (s, H8), 2.49 (sept, $^3J_{H6-H7}$ = 6.9, H6), 2.74 (sept, $^3J_{H16'-H17'(H18')}$ = 6.6, H16′), 3.71 (sept, $^3J_{H16-H17(H18)}$ = 6.6, H16), 4.65 (dd, $^3J_{H2-H3}$ = 6.0, $^4J_{H2-H6}$ = 1.0, H2), 4.67 (dd, $^3J_{H3'-H2'}$ = 5.9, H3′), 5.20 (dd, $^3J_{H2'-H3'}$ = 6.2, $^4J_{H2'-H6}$ = 1.1, H2′), 5.26 (dd, $^3J_{H3-H2}$ = 6.0, $^4J_{H3-H5}$ = 0.7, H3 (**a**)), 6.80 (dd, $^3J_{H11'-H12'}$ = 8.1, $^4J_{H11'-H13'}$ = 1.2, H11′) 6.90 (t, $^3J_{p-m}$ = 7.32, *p*), 7.03, (t, $^3J_{m-o,p}$ = 7.41, *m*), 7.31 (br, *o*), 7.46 (m, and H12 or H12′), 7.59 (m, H13, H13′ and H14), 7.70 (d, $^3J_{H14'-H13'}$ = 7.5, H14′), 7.87 (dd, $^3J_{H11'-H12'}$ = 8.1, $^4J_{H11'-H13'}$ = 1.2, H11′). Anal. Calcd (%) for $C_{56}H_{62}BClN_2Ru$ (910.4): C 73.88, H 6.86, N 3.08. Found: C 73.80, H 6.82, N 3.04.

4PF$_6$. ^1H NMR ($CDCl_3$, 298 K, 400.13 MHz, *J* values in Hz): δ 1.07 ((d, $^3J_{H18-H16}$ = 6.67, H18(**a**)), 1.08 (d, $^3J_{H7'-H6}$ = 6.78, H7′(**a**)), 1.11 (d, $^3J_{H7-H6}$ = 6.93, H7(**s**)), 1.17 (d, $^3J_{H7-H6}$ = 6.98, H7(**a**)), 1.37 (m, H17 and H18′(**a**) and H18(**s**)), 1.52 (d, $^3J_{CH3-CH}$ = 6.86, H18(**s**)), 1.53 (d, $^3J_{CH3'-CH'}$ = 6.67, 17′(**a**)), 1.82 (s, H5-(**s**)), 2.02 (s, H5(**a**)), 2.23 (sept, $^3J_{H6-H7}$ = 6.84, H6(**s**)), 2.30 (s, H8′(**a**)), 2.33 (s, H8(**s**)), 2.34 (s, H8(**a**)), 2.54 (sept, $^3J_{H6-H7}$ = 6.90, H6(**a**)), 2.90 (sept, $^3J_{H16-H17(H18)}$ = 6.67, H16 (**s**)), 3.08 (sept, $^3J_{H16'-H17'(H18')}$ = 6.58, H16′(**a**)), 3.74 (sept, $^3J_{H16-H17(H18)}$ = 6.77, H16(**a**)), 4.61 (dd, $^3J_{H2'-H3'}$ = 6.02, $^4J_{H2'-H6}$ = 1.02, H2′(**a**)), 4.74 (dd, $^3J_{H3-H2}$ = 5.93, H3(**a**)), 5.06 (d, $^3J_{H2-H3}$ = 6.25, H2(**s**)), 5.13 (dd, $^3J_{H2-H3}$ = 6.25, $^4J_{H2-H6}$ = 1.09, H2(**a**)), 5.28 (d, $^3J_{H8-H2}$ = 6.28, H3(**s**)), 5.41 (dd, $^3J_{H3'-H2'}$ = 6.05, $^4J_{H3'-H5}$ = 0.70, H3′(**a**)), 7.34 (m, H12(**s**) and H12 or H12′(**a**)), 7.46 (m, H13 and H13′(**a**) and H12 or H12′(**a**)), 7.53 (m, H11(**a**) and H13(**s**)), 7.59 (m, H14-(**s**) and H14 and H14′(**a**)), 7.80 (dd, $^3J_{H11-H12}$ = 8.06, $^4J_{H11-H13}$ = 1.22, H11(**s**)), 7.87 (dd, $^3J_{H11'-H12'}$ = 8.10, $^4J_{H11'-H13'}$ = 1.23, H11′(**a**)). ^{19}F NMR (CD_2Cl_2, 298 K): δ −72.1 (d, $^1J_{FP}$ = 711). ^{31}P NMR (CD_2Cl_2, 298 K): δ −143.2 (sept, $^1J_{PF}$ = 711). Anal. Calcd (%) for $C_{32}H_{42}ClF_6N_2PRu$ (736.2): C 52.21, H 5.75, N 3.81. Found: C 52.28, H 5.71, N 3.85.

4BF$_4$ *anti*. ^1H NMR (CD_2Cl_2, 298 K, 400.13 MHz, *J* values in Hz): δ 1.07 (d, $^3J_{H18-H16}$ = 6.67, H18), 1.08 (d, $^3J_{H7'-H6}$ = 6.78, H7′), 1.18 (d, $^3J_{H7-H6}$ = 6.98, H7), 1.34 (d, $^3J_{CH18-H16}$ = 3.51, H18), 1.40 (d, $^3J_{CH17'-H16}$ = 3.51, H17′), 1.54 (d, $^3J_{CH17-H16}$ = 3.51, H17), 2.01 (s, H5), 2.29 (s, H8), 2.32 (s, H8′), 2.50 (sept, $^3J_{H6-H7}$ = 6.84, H6), 2.34 (s, H8), 2.90 (sept, $^3J_{CH-CH3}$ = 6.67, CH(**s**)), 3.04 (sept, $^3J_{H16-H17(H18)}$ = 6.58, H16), 3.79 (sept, $^3J_{H16'-H17'(H18')}$ = 6.58, H16′), 4.66 (d, $^3J_{H2'-H3'}$ = 6.25, H2′), 4.73 (d, $^3J_{H3'-H2'}$ = 6.25, H3′), 5.21 (d, $^3J_{H2-H3}$ = 6.28, H2), 5.40 (d, $^3J_{H3'-H2'}$ = 6.05, H3′), 7.38 (m, H11′,H12, and H12′), 7.52 (m, H13 and H13′), 7.62 (m, H14 and H14′), 7.82 (dd, $^3J_{H11'-H12'}$ = 8.10, $^4J_{H11'-H13'}$ = 1.23, H11′). ^{19}F NMR (CD_2Cl_2, 298 K): δ −151.8 (br, $^{10}BF_4$), −151.9 (br, $^{11}BF_4$). Anal. Calcd (%) for $C_{32}H_{42}BClF_4N_2Ru$ (678.0): C 56.69, H 6.24, N 4.13. Found: C 56.61, H 6.28, N 4.18.

5PF$_6$. ^1H NMR ($CDCl_3$, 298 K, 400.13 MHz, *J* values in Hz): δ 2.34 (s, 8), 5.27 (s, benzene), 7.71−7.67 (m, 11−15). ^{19}F NMR (CD_2Cl_2, 298 K): δ −72.1 (d, $^1J_{FP}$ = 711). ^{31}P NMR (CD_2Cl_2, 298 K): δ −143.2 (sept, $^1J_{PF}$ = 711). Anal. Calcd (%) for $C_{22}H_{22}ClF_6N_2PRu$ (595.9): C 44.34, H 3.72, N 4.70. Found: C 44.39, H 3.75, N 4.73.

NOE Measurements. The ^1H-NOESY[29] NMR experiments were acquired by the standard three-pulse sequence or by the PFG version.[30] Two-dimensional $^{19}F-^1H$-HOESY NMR experiments were acquired using the standard four-pulse sequence or the modified version.[31] The number of transients and the number of data points were chosen according to the sample concentration and the desired final digital resolution. Semiquantitative spectra were acquired using a 1 s relaxation delay and 800 ms mixing time. Quantitative ^1H-NOESY and $^1H-^{19}F$-HOESY NMR experiments were carried out with a relaxation delay of 7 s and a mixing time of 0.15 s (initial rate approximation).[32]

PGSE Measurements. All the PGSE NMR measurements were performed by using the standard stimulated echo pulse sequence[33] on a Bruker AVANCE DRX 400 spectrometer equipped with a GREAT 1/10 gradient unit and a QNP probe with a Z-gradient coil, at 296 K without spinning.

The dependence of the resonance intensity (**I**) on a constant waiting time and on a varied gradient strength (**G**) is described by eq 2:

$$\ln \frac{I}{I_0} = -(\gamma\delta)^2 D_t\left(\Delta - \frac{\delta}{3}\right)G^2 \qquad (2)$$

where I = intensity of the observed spin echo, I_0 = intensity of the spin echo without gradients, D_t = diffusion coefficient, Δ = delay between the midpoints of the gradients, δ = length of the gradient pulse, and γ = magnetogyric ratio.

The shape of the gradients was rectangular, their duration (δ) was 4−5 ms, and their strength (G) was varied during the experiments. All the spectra were acquired using 32K points and a spectral width of 5000 (^1H) and 18000 (^{19}F) Hz and were processed with a line broadening of 1.0 (^1H) and 1.5 (^{19}F) Hz. After having checked that a change in total relaxation time (from 5 to 130 s) did not affect the measurement results, standard experiments were carried out with a total recycle time of 5 s. The semilogarithmic plots of $\ln(I/I_0)$ versus G^2 were fitted using a standard linear regression algorithm, and an R factor better than 0.99 was always obtained. Different values of Δ, "nt" (number of transients), and number of different gradient strengths (G) were used for different samples.

The self-diffusion coefficient, D_t, that is directly proportional to the slope of the regression line obtained by plotting $\log(I/I_0)$ versus G^2 (eq 2) was estimated by measuring the proportionality constant, using a sample of HDO (5%) in D_2O (known diffusion coefficient in the range 274−318K)[34] in the same exact conditions as the sample of interest using TMS as internal standard.[35] D_t data were treated as described in the literature.[6]

(29) Jeener, J.; Meier, B. H.; Bachmann, P.; Ernst, R. R. *J. Chem. Phys.* **1979**, *71*, 4546.
(30) Wagner, R.; Berger, S. *J. Magn. Reson. A* **1996**, *123*, 119.
(31) Lix, B.; Sönnichsen, F. D.; Sykes, B. D. *J. Magn. Reson. A* **1996**, *121*, 83.
(32) Neuhaus, D.; Williamson, M. *The Nuclear Overhauser Effect in Structural and Conformational Analysis*; Wiley-VCH: New York, 2000; Chapter 4.
(33) Valentini, M.; Rüegger, H.; Pregosin, P. S. *Helv. Chim. Acta* **2001**, *84*, 2833, and references therein.
(34) (a) Tyrrell, H. J. W.; Harris, K. R. *Diffusion in Liquids*; Butterworth: London, 1984. (b) Mills, R. *J. Phys. Chem.* **1973**, *77*, 685.

Table 6. Crystallographic Data for 1BPh$_4$, 2BF$_4$ *syn*, 3BPh$_4$ *anti*, 4BPh$_4$ *anti*, and 5PF$_6$

	1BPh$_4$·CH$_2$Cl$_2$	**2**BF$_4$ *syn*	**3**BPh$_4$ *anti*·CH$_2$Cl$_2$	**4**BPh$_4$ *anti*·CH$_3$OH	**5**PF$_6$
formula	$C_{51}H_{52}BCl_3N_2Ru$	$C_{28}H_{34}BClF_4N_2Ru$	$C_{55}H_{60}BCl_3N_2Ru$	$C_{57}H_{66}BClN_2ORu$	$C_{22}H_{22}ClN_2RuPF_6$
M	911.18	621.90	924.82	942.45	595.91
T [K]	295(2)	295(2)	295(2)	295(2)	298(2)
color	red	orange	yellow	yellow	orange
cryst syst	orthorhombic	monoclinic	orthorhombic	monoclinic	triclinic
space group	*Pbca*	$P2_1/a$	$P2_1/b2/c2_1/n$	$P2_1/c$	$P\bar{1}$
a [Å]	14.634(4)	17.250(5)	19.726(5)	15.378(5)	10.028(5)
b [Å]	21.829(6)	11.526(6)	16.920(5)	19.605(6)	10.494(5)
c [Å]	29.141(4)	17.310(4)	28.889(5)	17.284(5)	12.573(6)
α [deg]	90.00	90.00	90.00	90.00	69.207(4)
β [deg]	90.00	113.19(5)	90.00	104.61(5)	73.318(5)
γ [deg]	90.00	90.00	90.00	90.00	81.083(6)
V [Å^3]	9309(4)	3163.6(22)	9642(4)	5042(3)	1182.8(10)
Z	8	4	8	4	2
ρ_{calcd} [g cm^{-3}]	1.300	1.306	1.274	1.241	1.673
R_{int}	0.0590	0.0662	0.0674	0.0621	0.0511
GOF	0.970	1.035	1.121	0.990	1.145

The measurement uncertainty was estimated by determining the standard deviation of *m* by performing experiments with different Δ values. Standard propagation of error analysis yielded a standard deviation of approximately 3−4% in the hydrodynamic radius and 10−15% in the aggregation numbers *N*.

Computational Details. All calculations were performed with the Gaussian 03 set of programs[36] with DFT or the hybrid ONIOM method.[37] The cation **3**$^+$ *anti* and *syn* were optimized at the B3PW91 level.[38] The ion pair complexes for **3**X *anti* (X = BF$_4$ and BPh$_4$) with X close to the diimine methyl groups (**3**X-B) or above the cymene ring (**3**X-A) were optimized at the ONIOM-(B3PW91/HF) and ONIOM(B3PW91/UFF) levels. The UFF force field[39] was used for the molecular mechanics calculations. For the cationic fragment of **3**X *anti*, the isopropyl and methyl groups on cymene, as well as the ethyl-substituted phenyl groups of the diimine ligand, were considered in the low-level layer (HF or UFF). All of the remaining atoms were treated at the B3PW91 level. The BF$_4$ was treated at the B3PW91 level, and the phenyl groups on BPh$_4$ were considered in the low-level layer (HF or UFF).

In the B3PW91 calculations and in the high-level layer of the ONIOM calculations, the ruthenium atom was represented by the relativistic effective core potential (RECP) from the Stuttgart group (16 valence electrons) and its associated (8s7p5d)/[6s5p3d] basis set[40] augmented by an f polarization function (α = 1.235). The chloride atom was also treated with Stuttgart's RECPs and the associated basis set[41] augmented by a polarization d function (α = 0.640). For the remaining atoms 6-31G(d,p) basis sets were considered. For the calculations at the HF level in the ONIOM calculations, the ruthenium and chloride atoms were described by the Hay and Wadt pseudopotential and the associated basis sets.[42] The remaining atoms were represented by 4-31G basis sets. Full optimizations of geometry without any constraint were performed, followed by analytical computation of the Hessian matrix to confirm the nature of the located extrema as minima on the potential energy surface. The ion pair energies and the formation energy of the ion pair from separated anion and cation, as well as the relative energies and formation energies of the quadrupole from the separated ion pairs, were estimated through PCM calculations[43] in CH$_2$Cl$_2$ on the ONIOM(B3PW91/HF) geometries (ion pair) or B3PW91 geometries (quadrupole). In each case the geometries of the separated species (cation or anion for ion pair or ion pair for quadrupole) were not reoptimized but were taken as in the corresponding aggregate (ion pair or quadrupole).

X-ray Structure. A single crystal of **1**BPh$_4$, **2**BF$_4$ *syn*, **3**BPh$_4$ *anti*, **4**BPh$_4$ *anti*, and **5**PF$_6$ suitable for X-ray diffraction was obtained as described in the Experimental Section for each complex. Data were collected on an XCALIBUR (CCD areal) Oxford Instruments diffractometer, using Mo K graphite-monochromated radiation (λ = 0.71073 Å). ω, ϕ scans and the frame data were acquired with CRYSALIS (CCD 171) software. The crystal to detector distance was 65.77 mm. The frames of a single experiment were processed using CRYSALIS (RED 171) software to give the respective *hkl* file corrected for scan speed, background, Lorentz, and polarization affects. Since there were no apparent variations in the intensity of the standard reflections of all compounds, measured periodically, during data collection, no correction for crystal decomposition was necessary. The data were corrected for absorption using the semiempirical multiscan sistem.[44] The Laue symmetry was determined for all compounds, and the investigations of the observed systematic absences were consistent with the assigned space groups. All of the data were collected at room temperature.

The structures were solved by the direct method using the Sir97[45] program and refined by the full-matrix least-square method on F^2

(35) Babushkin, D. E.; Brintzinger, H. H. *J. Am. Chem. Soc.* **2002**, *124*, 12869.

(36) Frisch, M. J.; Trucks, G. W.; Schlegel, H. B.; Scuseria, G. E.; Robb, M. A.; Cheeseman, J. R.; Montgomery, J. A., Jr.; Vreven, T.; Kudin, K. N.; Burant, J. C.; Millam, J. M.; Iyengar, S. S.; Tomasi, J.; Barone, V.; Mennucci, B.; Cossi, M.; Scalmani, G.; Rega, N.; Petersson, G. A.; Nakatsuji, H.; Hada, M.; Ehara, M.; Toyota, K.; Fukuda, R.; Hasegawa, J.; Ishida, M.; Nakajima, T.; Honda, Y.; Kitao, O.; Nakai, H.; Klene, M.; Li, X.; Knox, J. E.; Hratchian, H. P.; Cross, J. B.; Bakken, V.; Adamo, C.; Jaramillo, J.; Gomperts, R.; Stratmann, R. E.; Yazyev, O.; Austin, A. J.; Cammi, R.; Pomelli, C.; Ochterski, J. W.; Ayala, P. Y.; Morokuma, K.; Voth, G. A.; Salvador, P.; Dannenberg, J. J.; Zakrzewski, V. G.; Dapprich, S.; Daniels, A. D.; Strain, M. C.; Farkas, O.; Malick, D. K.; Rabuck, A. D.; Raghavachari, K.; Foresman, J. B.; Ortiz, J. V.; Cui, Q.; Baboul, A. G.; Clifford, S.; Cioslowski, J.; Stefanov, B. B.; Liu, G.; Liashenko, A.; Piskorz, P.; Komaromi, I.; Martin, R. L.; Fox, D. J.; Keith, T.; Al-Laham, M. A.; Peng, C. Y.; Nanayakkara, A.; Challacombe, M.; Gill, P. M. W.; Johnson, B.; Chen, W.; Wong, M. W.; Gonzalez, C.; Pople, J. A. *Gaussian 03*, Revision C.02; Gaussian, Inc.: Wallingford, CT, 2004.

(37) Svensson, M.; Humbel, S.; Froese, R. D. J.; Matsubara, T.; Sieber, S.; Morokuma, K. J. *J. Phys. Chem.* **1996**, *100*, 19357.

(38) (a) Becke, A. D. J. *J. Chem. Phys.* **1993**, *98*, 5648. (b) Perdew J. P.; Wang, Y. *Phys. Rev. B* **1992**, *45*, 13244.

(39) Rappe, A. K.; Casewitt, C. J.; Colwell, K. S.; Goddard W. A.; Skiff, W. M. *J. Am. Chem. Soc.* **1992**, *114*, 10024.

(40) Andrae, D.; Häussermann, U.; Dolg, M.; Stoll, H.; Preuss, H. *Theor. Chim. Acta* **1990**, *77*, 123.

(41) Bergner, A.; Dolg, M.; Küchle, W.; Stoll, H.; Preuss, H. *Mol. Phys.* **1990**, *30*, 1431.

(42) (a) Wadt, W. R.; Hay, P. J. *J. Chem. Phys.* **1985**, *82*, 284. (b) Hay, P. J. Wadt, W. R. *J. Chem. Phys.* **1985**, *82*, 299.

(43) Tomasi, J.; Mennucci, B.; Cammi, R. *Chem. Rev.* **2005**, *105*, 2999.

(44) Blessing, R. H. *Acta Crystallogr.* **1995**, *A51*, 33.

(45) Altomare, A.; Burla, M. C.; Camalli, M.; Cascarano, G.; Giacovazzo, C.; Gagliardi, A.; Moliterni, A. G. G.; Polidori, G.; Spagna, R. *J. Appl. Crystallogr.* **1999**, *32*, 115.

using SHELXL-97[46] WinGX[47]. All non-hydrogen atoms were refined anisotropically. The hydrogen atoms were added at the calculated positions and refined using a riding model. The final cycles of full-matrix least-squares refinement against F^2 were based on the observed reflections with $[F_o > 4\sigma(F_o)]$ and were converged with unweighted and weighted agreement factors of R and R_w and GOF. Crystals of **1**BPh_4, **3**BPh_4 *anti*, and **4**BPh_4 *anti* showed internal disorder due to a solvent molecule that cocrystallized with the complexes. Crystallographic details are summarized in Table 6.

Acknowledgment. This work was supported by grants from the Ministero dell'Istruzione, dell'Università e della Ricerca (MIUR, Rome, Italy; Programma di Rilevante Interesse Nazionale, Cofinanziamento 2004-2005), COST D24/WG 0014/02 action, Université Montpellier 2 and CNRS.

Supporting Information Available: This material is available free of charge via the Internet at http://pubs.acs.org.

OM7003157

(46) Sheldrick, G. M. *SHELXL-97*, Release 92-2; A program for crystal structure refinement; University of Goettingen: Germany, 1997.

(47) Farrugia, L. J. *J. Appl. Crystallogr*. **1999**, *32*, 837.